ZIP9 is a Druggable Determinant of Sex Differences in Melanoma

Cristina Aguirre-Portolés[1], Riley Payne[2], Aspen Trautz[1], J. Kevin Foskett[2], Christopher A. Natale[1], John T. Seykora[1], Todd W. Ridky[1]*

[1]Department of Dermatology, Perelman School of Medicine, University of Pennsylvania.
[2]Department of Physiology, Perelman School of Medicine, University of Pennsylvania, Philadelphia, PA. USA.
*Correspondence to: ridky@pennmedicine.upenn.edu

Abstract

Melanoma and most other cancers occur more frequently, and have worse prognosis, in males compared with females. Though sex steroids are thought to be involved, classical androgen and estrogen receptors are not detectable in most melanomas. Here we show that testosterone promotes melanoma proliferation by activating ZIP9 (*SLC39A9*), a zinc transporter that is not intentionally targeted by available therapeutics, but is widely expressed in human melanoma. This testosterone activity requires zinc influx, MAPK activation and YAP1 nuclear translocation. We demonstrate that FDA approved inhibitors of the classical androgen receptor also inhibit ZIP9, and thereby antagonize the pro-tumorigenic effects of testosterone in melanoma. In male mice, androgen receptor inhibitors suppressed growth of ZIP9-expressing melanomas, but had no effect on isogenic melanomas lacking ZIP9, nor on melanomas in females. These data suggest that ZIP9 might be effectively targeted in melanoma and other cancers by repurposing androgen receptor inhibitors that are currently approved only for prostate cancer.

Conflict of interest

T.W.R., C.A.N and C.A.P. are inventors on a provisional patent held by the University of Pennsylvania related to this work.

30 **Introduction**

31

32 Cancer incidence and mortality are higher in males than in females in the U.S. and worldwide[1,2].
33 In the U.S., males are 15% more likely to develop cancer, and 40% more likely to die from this
34 disease than females[1]. These sex differences were recognized as early as 1949[3], are observed in
35 the majority of cancer types from non-reproductive tissues[1], and remain even after controlling for
36 known risk factors such as environmental and occupational exposures[4]. While recent advances in
37 modern targeted and immune therapeutics have markedly improved survival for both female and
38 male melanoma patients[5], females still have more favorable outcomes[1,4]. Defining the
39 mechanisms underlying the broad and persistent sex differences in cancer incidence and
40 outcomes will address a major unresolved question in cancer pathobiology.

41 We previously showed that the female sex hormone estradiol inhibits melanoma
42 proliferation and tumor growth *in vivo*. This effect is independent of biologic sex of the tumor,
43 independent of classical estrogen receptors (ER), and results from activation of a nonclassical
44 surface estrogen receptor on melanocytes and melanoma cells called the G Protein Estrogen
45 Receptor (GPER)[6,7]. This work led us to consider whether male sex hormone signaling might
46 also contribute to female vs. male differences in melanoma progression.

47 Testosterone is the most abundant androgen and circulates at much higher levels in
48 males (630 ng/dl) than in females (32 ng/dl)[8]. In males, higher levels of circulating testosterone
49 also correlate with increased melanoma incidence[9]. Testosterone promotes proliferation *in vitro*
50 in non-gonadal cell types including adipocytes[10], mouse skeletal muscle myoblasts[11],
51 glioblastoma-derived cells[12], lung cancer cell lines[13] and melanoma[14]. As the classical androgen
52 receptor (AR) is not consistently detected in most of these tissues, the receptor(s) mediating the
53 testosterone-dependent increased proliferation and the corresponding downstream mechanisms

54 are not yet defined. Also unknown is whether this androgen activity observed *in vitro* is relevant
55 to cancer progression *in vivo*.

56 Here we studied 98 human melanocytic lesions (nevus, primary and metastatic melanoma
57 from both males and females) and did not detect AR in any of them. However, in nearly all
58 samples, we readily detected ZIP9, a membrane localized zinc transporter recently discovered in
59 Atlantic Croaker (fish) cells to be a activated by testosterone[19].

60 Here, we use genetic and pharmacologic approaches to target ZIP9 in multiple melanoma
61 models in vitro and in vivo. These functional studies define a previously unappreciated
62 nonclassical testosterone signaling pathway through ZIP9, establish a novel mechanistic link
63 between male androgens and melanoma pathobiology, and highlight a potential new therapeutic
64 opportunity by repurposing currently available drugs.

65

66 **Results**

67

68 **Melanoma tumors grow more quickly in male vs. female mice**.

69

70 To test whether preclinical melanoma models recapitulate the male vs. female survival disparity
71 observed in humans, we first determined growth of human BRAF-driven melanoma (WM46,
72 female origin, $BRaf^{V600E}$; $CDK4^{R24C}$). Tumors grew faster in immunodeficient SCID male mice
73 compared with matched female mice (Fig. 1A and Fig. S1A), indicating that the differences do
74 not depend on T and/or B cell immune responses. To test whether this phenotype extends to a
75 genetically-engineered preclinical mouse model, we used murine YUMM1.7 cells (male origin,
76 $BRaf^{V600E/wt}$;$Pten^{-/-}$$CdkN2a^{-/-}$)[16] in syngeneic immunocompetent C57BL/6 mice. These tumors
77 also consistently grew faster in male mice compared with matched females (Fig. S1B).

78

79 **Testosterone, but not dihydrotestosterone, promotes proliferation in melanoma cells**
80 **independent of the classical androgen receptor.**

81 Physiologic concentrations of testosterone promoted proliferation of both normal early passage
82 primary human melanocytes and melanoma cells (Fig. 1B, C and Fig. S1C). The proliferative
83 response to testosterone correlated with dose and was saturable, suggesting a specific receptor-
84 mediated activity. In contrast, dihydrotestosterone (DHT) had no effect on proliferation of these
85 cell types across a wide concentration range (Fig. 1C). Dihydrotestosterone is a more potent AR
86 agonist than testosterone[17,18]. The fact that the melanocytes and melanoma cells responded to
87 testosterone, but not to DHT (Fig. 1B, 1C, Fig. S1C, S1D and S1E), suggests the possibility that
88 testosterone effects in these cells are mediated by the nonclassical androgen receptor ZIP9, as
89 ZIP9 has a much higher affinity for testosterone than for dihydroteststerone[19]. Further suggesting
90 the idea that a nonclassical androgen receptor mediates these observed testosterone effects, we
91 were unable to detect AR protein (via western blotting using 2 different AR antibodies, or via
92 immunofluorescence, Table S1) in primary melanocytes, or in any of the 8 melanoma cell lines
93 we have tested. We did however, readily detect AR protein in 3 prostate cancer lines used as
94 positive controls (Fig. 1D and Fig. S1F and S1G). Consistent with this lack of detectable AR
95 protein, AR transcript was not detected via RNASeq in any of 6 different primary human
96 melanocyte cultures. In contrast, *SLC39A9*/ZIP9 transcript, as well as transcript for the classical
97 nuclear glucocorticoid receptor *NR3C1*, and for the melanocyte marker *MC1R*, were each readily
98 detected in all the cell lines (Fig. 1E).

99 To test whether testosterone effects in melanoma cells are mediated by a surface receptor,
100 we next treated WM46 and SK-MEL-24 human melanoma cells, (female and male derived,
101 respectively) with a membrane-impermeable testosterone analogue [(Testosterone 3-(O-

102 carboxymethyl)oxime: BSA] that is incapable of activating AR (AR is necessarily active in the
103 nucleus). This compound and free testosterone each similarly promoted melanoma proliferation
104 (Fig. S2A), supporting the idea that a non-classical androgen receptor located in the cellular
105 membrane was responsible for the observed phenotype.

106 ZIP9 is broadly expressed in most cancers (Fig. S2B), normal human melanocytes, and
107 all melanoma lines that we tested (Fig. 2A). ZIP9 transports zinc (Zn^{++}) across cell and organelle
108 membranes into the cytoplasm and is the only steroid receptor known to directly regulate zinc
109 homeostasis[20]. To test whether testosterone activates this ZIP9 activity in melanoma, we used the
110 fluorescent Zn^{++}-specific probe FluoZin-3. Testosterone induced a rapid increase in cytosolic
111 free Zn^{++} ($[Zn^{++}]_i$) in human melanoma cells (Fig. 2B), that was followed by a sustained
112 elevation for at least 2 days in the presence of testosterone (Fig. 2C). We determined that Zn^{++}
113 influx was necessary for the testosterone-dependent increase in melanoma cell proliferation, as
114 treatment with the Zn^{++} chelator N,N,N′,N′-tetrakis (2-pyridinylmethyl)-1,2-ethanediamine
115 (TPEN), blocked testosterone induced proliferation at TPEN concentrations that had no
116 significant effect on proliferation when used alone (Fig. 2D and Fig. S2C).

117 Although TPEN has high affinity for Zn^{++}, it also has some ability to chelate copper[21]. To
118 test whether copper flux might contribute to testosterone effects on melanoma proliferation, we
119 treated WM46 cells with $CuSO_4$, which had no significant effect on cell proliferation (Fig. S2D).
120 Moreover, the highly specific copper chelator bathocuproinedisulfonic acid (BCS), did not affect
121 the proliferative response to testosterone, nor did BCS affect testosterone induced Zn^{++} influx
122 (Fig. S2E and Fig. S2F).

123 After determining that Zn^{++} influx was necessary for testosterone-induced proliferation,
124 we next tested whether increased Zn^{++} was sufficient to increase melanoma proliferation.

125 Exogenous zinc pyrithione (also a Zn^{++} ionophore), and $ZnCl_2$ each increased melanoma
126 proliferation (Fig. 2E). Other biologically-relevant divalent cations, Fe^{++} and Mn^{++}, known to be
127 transported by other ZIP family members[22], had no effect on proliferation (Fig. 2E). Together,
128 these results demonstrate that testosterone, but not DHT, promotes zinc dependent proliferation
129 in melanoma cells that express ZIP9 and lack detectable AR.

130 We next used immunocytochemistry to test whether AR and/or ZIP9 protein are
131 expressed in human melanocytic lesions (14 benign nevi, 63 primary melanomas, and 21
132 metastatic melanomas from both males and females). AR was determined in tissue sections using
133 a highly validated CLIA (Clinical Laboratory Improvement Amendments) certified method in
134 the clinical pathology lab at the Hospital of the University of Pennsylvania. This procedure uses
135 a validated antibody different from the two we used for western blotting and
136 immunofluorescence. Each tissue was scored in a blinded fashion by a board-certified
137 pathologist. While AR was readily detectable in prostate tissue used as positive control, AR was
138 not detected in any of the nevi, nor in the melanomas (Fig. 2F). In parallel, we analyzed the same
139 samples for ZIP9. CLIA grade ZIP9 IHC is not available. However, we validated our ZIP9
140 antibody using parental WM46 ZIP9 positive (wtZIP9) and isogenic ZIP9 negative (ΔZIP9) cell
141 lines. These cells were grown on chamber slides and processed for IHC in parallel with the
142 human samples. The antibody used labeled only the wtZIP9 cells. ZIP9 protein was observed in
143 100% of the nevi, 97% of primary melanomas and 100% of the metastatic samples (Fig. 2G).
144 Further, ZIP9 relative staining intensity positively correlated with tumor stage (Fig. 2H). No
145 significant differences in ZIP9 staining were observed between males and females (Fig. S2G).

146 We next questioned whether ZIP9 expression correlates with clinical melanoma
147 outcomes in people. We used *OSskm*[23] to analyze pooled data from 1085 tumors (563 death

148 events) from multiple studies (GSE17275, GSE19234, GSE22155_GPL6102,
149 GSE22155_GPL6947, GSE50509, GSE46517, GSE53118, GSE65904, GSE98394 and TCGA.
150 High ZIP9 expression associated with shorter survival (HR=1.2039) (Fig S2H), consistent with
151 the idea that ZIP9 promotes melanoma progression.
152
153 **Testosterone signaling through ZIP9 promotes melanoma growth**
154 To determine whether ZIP9 mediates testosterone effects, we used CRISPR-Cas9 and gRNA
155 targeting Slc39A9 exon 1 to ablate ZIP9 in human (WM46) melanoma and in murine
156 (YUMM1.7) melanoma. Isogenic clonal populations of parental ZIP9-expressing (wtZIP9) and
157 ZIP9-ablated (ΔZIP9) cells were established, and the mutations disrupting the reading frame
158 were mapped by sequencing (Fig. S3A, S3B and S3C). ZIP9 protein was not detectable in ΔZIP9
159 cells (Fig. 2F, Fig. 3A, Fig. 3B and Fig. S3D). ΔZIP9 cells did not respond to testosterone,
160 whereas isogenic wtZIP9 control clones responded similarly to the parental wtZIP9 cells (Fig.
161 3A, 3B and Fig. S3E).
162 The testosterone insensitive phenotype associated with CRISPR-Cas9 engineered ZIP9 loss
163 was rescued by expression of a human ZIP9 transgene. Lentiviral mediated constitutive ZIP9
164 expression in the ΔZIP9 WM46 cells restored both ZIP9 protein and the proliferative response to
165 testosterone, verifying the on-target effects of the CRISPR-Cas9 mediated ZIP9 ablation (Fig.
166 S3F, S3G).
167 Consistent with the conclusion that ZIP9 is the major mediator of testosterone and
168 exogenous zinc effects in these melanoma cells, exposure to testosterone or to extracellular zinc
169 failed to increase $[Zn^{++}]_i$ in ΔZIP9 cells (Fig. 3C and 3D). Therefore, testosterone induces a

170 rapid, ZIP9-dependent, increase in $[Zn^{++}]_i$ that is required for the increased proliferation in
171 melanoma cells.
172
173 **Testosterone-induced melanoma proliferation through ZIP9 requires downstream MAPK**
174 **and YAP1 activation**
175 Although the studies detailed above show that testosterone promotes melanoma proliferation via
176 ZIP9 dependent Zn^{++} influx, zinc is involved in myriad cellular processes, making it difficult to
177 predict *a priori* which downstream signaling pathways are required for the testosterone activity.
178 To start identifying these, we used a 447-element Reverse Phase Protein Array (RPPA) analysis
179 of human WM46 melanoma cells treated with testosterone for 0, 30, 60 and 480 min. While the
180 relative expression of most represented proteins was unaffected by testosterone, some were
181 significantly under or overexpressed, including several with known tumor-promoting or tumor-
182 suppressive functions (Fig. 4A and Table S2). Downregulated proteins included 14-3-3ε, a tumor
183 suppressor and negative YAP1 regulator previously implicated in liver, lung, and gastric
184 cancers[24], and CDKN2A (p16), a cyclin-dependent kinase (CDK) inhibitor, and one of the most
185 studied tumor suppressors[25]. Upregulated proteins included key elements of tumor-promoting
186 pathways, most notably phosphorylated ERK (T202; Y204) and YAP1 (Fig. 4A).
187 Importantly, ΔZIP9 cells displayed decreased basal levels of ERK phosphorylation compared
188 with isogenic wild-type clones (Fig. S4A). MAPK activation was necessary for the testosterone-
189 dependent proliferative response, as the specific ATP-competitive ERK1/2 inhibitor, ulixertinib[26]
190 (RVD-523; Ei) blocked the testosterone-dependent proliferative response, at ulixertinib
191 concentrations that had no effect on the basal proliferation rate when used alone (Fig. 4B).
192 Testosterone-dependent ZIP9 activation appeared to render WM46 cells more sensitive to

193 ulixertinib, as cell viability was compromised when they were treated with both testosterone and
194 RVD-523. This vulnerability to combination treatment seems to be specific and ZIP9 dependent,
195 as ΔZIP9 cells treated with both testosterone and ulixertinib proliferated at rates comparable to
196 controls (Fig. 4B).

197 We determined that YAP1 activation is also required for the augmented proliferative
198 response driven by testosterone. YAP1 is a transcriptional coactivator whose activity is largely
199 regulated by its localization[27]. Testosterone induced rapid YAP1 translocation from cytoplasm to
200 nucleus in human melanoma cells in a ZIP9-dependent manner (Fig. 4C, 4D and Fig. S4B).
201 YAP1 subcellular localization is controlled largely by LATS, which phosphorylates YAP1 at
202 Serine 127 and thereby retains YAP1 in the cytoplasm[28]. The YAP1 inhibitor dobutamine also
203 promotes phosphorylation of YAP at Ser127[29]. Consistent with this, the testosterone induced
204 YAP1 nuclear localization and increase in cell proliferation were both blocked by dobutamine,
205 while this compound had no significant effect on its own (Fig. 4D, and Fig. 4E). When ZIP9
206 expression was rescued via lentiviral transduction of a ZIP9 transgene to ΔZIP9 WM46 cells,
207 testosterone dependent YAP1 translocation into the nucleus was also restored (Fig. S4C).

208 Testosterone promotion of YAP1 activity was evidenced by increased expression of
209 several well-known YAP1 target genes including CDC6, CTGF, CYR61 and THBS1. As
210 expected, these testosterone-induced expression changes were also blocked by dobutamine (Fig.
211 4F).

212

213

214

215 **Pharmacologic ZIP9 blockade inhibits testosterone-driven melanoma proliferation and**
216 **melanoma tumor growth *in vivo.***

217 We next tested whether FDA-approved drugs could be repurposed to effectively target
218 ZIP9. Although specific ZIP9 inhibitors are not yet developed, molecular modeling and
219 competition assays with fluorescent-tagged testosterone suggest that the androgen receptor
220 inhibitor bicalutamide (BIC) competes with testosterone for ZIP9 binding to the same
221 extracellular pocket and thereby acts as a competitive ZIP9 antagonist[30]. Bicalutamide was
222 developed and approved for prostate cancer and has now been largely replaced by enzalutamide
223 (ENZ) and apalutamide (APA), which are structurally related analogs with higher affinity for the
224 androgen receptor and greater clinical efficacy against advanced prostate cancer[31,32].

225 While ZIP9 was not known to be an androgen receptor at the time these drugs were
226 developed, we show here that they are nonetheless effective inhibitors of testosterone effects in
227 melanoma cells that express ZIP9, but that lack detectable AR. Each compound completely
228 blocked testosterone-induced proliferation and MAPK activation in several melanoma cell lines
229 (Fig. 5A, 5B). Importantly, these agents alone (without testosterone) had no effect on cell
230 proliferation (Fig. S5A). The testosterone dependent increase of intracellular zinc was also
231 efficiently blocked by bicalutamide (Fig. S5B). Moreover, ΔZIP9 cells transduced to re-express
232 ZIP9, responded to testosterone, and this effect was again blocked by bicalutamide (Fig. S5C).

233 To further confirm that these pharmacologic agents work through ZIP9, we next used
234 cyproterone acetate (CPA), an anti-androgen that blocks the testosterone interaction with AR, but
235 that does not bind to ZIP9[33]. In our melanoma cells, up to a 20-fold molar excess of CPA did not
236 significantly inhibit testosterone effects on proliferation, consistent with the conclusion that AR
237 is not the major mediator of testosterone effects in these melanoma models (Fig. S5D).

238 To test whether these pharmacologic bicalutamide class AR inhibitors block the physical
239 interaction between testosterone and ZIP9 in melanoma, we performed direct binding assays
240 using a membrane-impermeable testosterone analogue (T-BSA-FITC). This reagent labels the
241 plasma membrane surface of wild-type ZIP9 expressing WM46 melanoma cells (Fig. 5C). This
242 membrane bound testosterone was displaced by apalutamide, demonstrating the specificity of the
243 interaction (Fig. 5C). Further demonstrating that the binding is ZIP9 specific, testosterone
244 localization at the plasma membrane was markedly reduced in ΔZIP9 cells (Fig. 5C) that did not
245 respond to testosterone, nor to APA in vitro (Fig. 5D).

246 Next, we tested whether apalutamide and related analogs inhibit melanoma *in vivo*. For
247 this, we introduced wtZIP9 or isogenic ΔZIP9 human WM46 melanoma into SCID mice. Once-
248 daily systemically administered apalutamide (20 mg/kg/day via oral gavage) significantly
249 suppressed growth of wtZIP9 tumors in male mice and extended survival (doubling time for
250 tumor growth was 11.1 days for vehicle treated males and 25.2 days for APA treated males) (Fig.
251 5E, Fig. S6A). Similar results were obtained when males were treated with bicalutamide
252 (30mg/kg/day) (Fig. 5F). Importantly, bicalutamide had no effect on wtZIP9 tumors in female
253 mice, nor on ΔZIP9 tumors (Fig. 5F, G, Fig. S6B and C). Together, these data show that ZIP9
254 promotes melanoma progression specifically in males.

255

256 **Discussion**

257

258 Although many have speculated that sex steroids contribute to sex differences in cancer
259 pathobiology, definitive functional studies are lacking, and the mechanisms by which they
260 contribute to the male-female cancer sex gap are largely unknown. The role of nonclassical
261 estrogen, progesterone, and testosterone receptors (GPER1, PAQR7, and ZIP9, respectively) in

262 cancer pathobiology has been largely unexplored. However, these are highly likely to be
263 significant contributors to sex specific pathobiology in melanoma (and other cancers) as each are
264 transcribed at much higher levels than the classical nuclear sex steroid receptors, most of which
265 are not detectable above background (Fig. S7).

266 Testosterone promoted proliferation of melanoma cells in a saturable and dose-dependent
267 manner. Curiously, the same cell lines did not respond to DHT, which is generally considered
268 the more biologically active androgen. DHT displays 4-fold increased affinity than testosterone
269 for AR, and it dissociates from AR three time slower than testosterone[18]. Lack of response to
270 DHT in melanoma is consistent with the absence of detectable AR expression in the models used
271 for this study, and is highly consistent with our genetic data showing that ZIP9, which has higher
272 affinity for testosterone vs. DHT, is an important mediator of testosterone effects.

273 We show that ZIP9 activation via testosterone binding promotes an increase in cytosolic
274 zinc in melanoma cells. The mammalian family of zinc transporters SLC39A comprises 14
275 members (ZIP1–14)[34] grouped into four subfamilies that were stablished according to their
276 amino acid sequence similarities. There may be roles for these other family members in some
277 cancers, as ZIP1 (SLC39A1, from ZIPII subfamily) has been associated with the regulation of
278 zinc uptake in prostate cancer cells[35]. However, this rapid increase of intracellular zinc through
279 ZIP1 appears to be AR dependent, as PC-3 cells only respond to testosterone after they are
280 transfected with exogenous AR. ZIP9 is unique member of ZIPI subfamily[36], and the only one
281 known to directly interact with testosterone.

282 There may be many drivers of the cancer sex gap in humans, including differences in
283 immune surveillance[37]. However, differences in immune surveillance do not appear to be a major
284 driver of the differences in the melanoma models used for this study, as tumors progressed faster

285 not only in male vs. female syngeneic immunocompetent mice, but also in human melanomas
286 grown in male vs. female SCID mice. Therefore, the testosterone effects on melanoma in these
287 models are dependent on ZIP9, but independent of B and T cell mediated anti-tumor activity.
288 Consistent with this, ZIP9 expressing tumors responded to bicalutamide and apalutamide in
289 SCID mice.

290 As ZIP9 is widely expressed in nearly all tissues, it may be a major determinant of the sex
291 disparity in outcomes not just for melanoma, but also for many other cancer types. Consistent
292 with this, we observed that testosterone promotes proliferation in many diverse cancer cell types,
293 and that this effect is blocked by bicalutamide (Fig. S8).

294 While this work clearly establishes a major role for ZIP9 in melanoma, we do recognize
295 the possibility that some melanoma cell lines, and perhaps even some human tumors, may
296 express a low level of AR that also impacts melanoma. However, any such tumor would still
297 likely also be affected by ZIP9. A recent report[15] also considered a possible role for testosterone
298 in melanoma and, consistent with our data, concluded that testosterone promotes melanoma
299 progression. Authors attributed this effect to the classical AR. However, that report did not
300 consider the nonclassical androgen receptor ZIP9. Critically, that study did not show that AR
301 was necessary for melanoma response to pharmacologic AR inhibitors, nor did it test whether
302 AR was a determinant of sex differences in melanoma.

303 The demonstration here that ZIP9 is pharmacologically accessible, suggests that ZIP9
304 may be a new eminently druggable therapeutic target (Fig. 6), and that currently approved
305 androgen receptor inhibitors might be useful alone, or in combination with current standard of
306 care therapeutics for a wide range of cancers, especially those that disproportionately affect
307 males.

308 **Materials and Methods**

309

310 **CRISPR-Cas9 mediated ablation of Slc39A9**

311 We used lentiviral transduction to deliver dox-inducible Cas9 and gRNA targeting exon 1 of
312 Slc39A9 in human WM46 and murine YUMM1.7 melanoma cells. Transduced cells were
313 selected with puromycin, and single cells subsequently isolated, expanded and examined for
314 ZIP9 protein expression, compared to clones isolated in parallel with no doxycycline treatment.
315 The following gRNA sequences were used (5'-3'):

316 hZIP9_gRNA_Fw caccgTTGGTGGGATGTTACGTGGC

317 hZIP9_gRNA_Rv aaacGCCACGTAACATCCCACCAAC

318 hZIP9_gRNA_Fw caccgCGTGGCCGGAATCATTCC

319 hZIP9_gRNA_Rv aaacGGAATGATTCCGGCCACG

320 To map the targeted sequencing, the region surrounding the gRNA target sequence was
321 amplified in both WM46 (282bp) and YUMM1.7 (259bp) isogenic clones. The following
322 primers were used (5'-3'): hZIP9_CRISPRmut_Fw:
323 TAAGCAGAATTCATGGATGATTTCATCTCC

324 hZIP9_CRISPRmut_Rv:TAAGTAAGTCCAAGCTTCTGCTGCTTTGTCTGATGCA.

325 mZIP9_CRISPRmut_F:TAAGCAGAATTCATGGATGACTTTCTCTC.

326 mZIP9_CRISPRmut_Rv TAAGTAAGTCCAAGCTTGATATTTCTGCTGCTTTGT.

327 Once amplified, DNA fragments were cloned into pUC19 vector using EcoRI and HindDIII
328 sites, and sequenced (Sanger) by the DNA Sequencing Facility (University of Pennsylvania).
329 Sequences were analyzed using the free software CRISP-ID (V1.1) and ICE Analysis by
330 Synthego were the knock-out scores were obtained.

331

332 **Cell culture and proliferation assays**

333 YUMM1.7, SH-4 and SK-MEL-2 cells were purchased from ATCC (YUMM1.7 ATCC® CRL-
334 3362™; SH-4 ATCC® CRL-7724™; SK-MEL-2 ATCC® HTB-68™) and cultured in DMEM
335 (Mediatech, Manassas, VA, USA) with 5% FBS (Invitrogen, Carlsbad, CA, USA) and 1%
336 Penicillin-Streptomycin (Thermo Fisher Scientific. #15140122). SK-MEL-3 cells were
337 purchased from ATCC (ATCC® HTB-69™ and cultured in McCoy's 5A (Modified) Medium
338 with 10% FBS (Invitrogen, Carlsbad, CA, USA) and 1% Penicillin-Streptomycin. SK-MEL-24
339 cells were purchased from ATCC (ATCC® HTB-71™) and cultured in Eagle's Minimum
340 Essential Medium with 15% FBS and 1% Penicillin-Streptomycin. WM46 melanoma cells were
341 a gift from Meenhard Herlyn (Wistar Institute, Philadelphia, PA, USA) and were cultured in
342 TU2% media. Tumor cells were regularly tested using MycoAlert Mycoplasma Detection Kit
343 from Lonza (Allendale, NJ, USA). Early passage cells were used after obtaining them directly
344 from ATCC. For monitoring cell proliferation $10x10^5$ YUMM1.7 or $12x10^5$ WM46 cells were
345 seed per well in 12-well Cell culture Plates. All the experiments performed in this work utilized
346 charcoal stripped serum (Fetal Bovine Serum, charcoal stripped, USDA-approved regions, One
347 Shot™ format. Catalogue number #A3382101; Thermofisher Scientific). Cells were treated
348 every second day and manually counted in triplicate using a hemocytometer (Testosterone
349 solution and Testosterone-CMO-BSA were purchased from Sigma-Aldrich, T5411-1ML and
350 T3392-10MG respectively). All the experiments were performed in cell populations that were in
351 culture during a maximum of 3 weeks (5 passages in average) since thaw from the corresponding
352 stock.

353

354

355 **Zinc influx analysis**

356 WM46 cells were loaded with 5 µM FluoZin™-3, AM cell permeant™ (Thermo Fisher
357 Scientific, #F24195), for 20 minutes then incubated in 2 Ca Tyrode's solution (in mM: 140
358 NaCl, 5 KCl, 1 $MgCl_2$, 2 $CaCl_2$, 10 glucose and 5 (Na) Pyruvate – pH 7.4) for 5-10 minutes at
359 room temperature prior to imaging. Cells were imaged on a Nikon Ti microscope using a
360 20x/0.75 NA objective for fluorescence at 340 nm and 380nm excitation/515 nm emission (Ca^{2+}-
361 free Fura2 or FluoZin™-3) and 380 nm excitation/515 nm emission (Ca^{2+}-free Fura2 FluoZin™-
362 3). Coverslips were perfused at 1-3 mL/min following this protocol: Ca^{2+} Tyrode's (0-30 secs);
363 Ca^{2+} Tyrode's + DMSO & 5 uM Zinc (30-90 secs); Ca^{2+} Tyrode's + Testosterone & 5µM Zinc
364 (90-360 secs); Ca^{2+} Tyrode's + Testosterone + BIC & 5 uM Zn (360-470 secs); Ca^{2+} Tyrode's
365 washout (470-500 secs). 100 milliseconds exposure images for each wavelength were collected
366 every 2 seconds. For analyzing the long-term consequences of testosterone treatment, cells were
367 treated with the androgen for 96 hours and then loaded FluoZin™-3. Cells were incubated with
368 FluoZin™-3 following manufacturer recommendation and exposed to 400nM Zn pyrithione or
369 $ZnCl_2$. Images were acquired with EVOS BLA. Fluorescence was quantitated using ImageJ
370 (National Institutes of Health, Bethesda, MD, USA), and statistical analyses were performed
371 using Graphpad Prism software.

372

373 **Reverse Phase Protein Array (RPPA)**

374 We used the Functional Proteomics Core at MD Anderson
375 (https://www.mdanderson.org/research/research-resources/core-facilities/functional-proteomics-
376 rppa-core.html) to perform a 447-element Reverse Phase Protein Array (RPPA) analysis of
377 human melanoma cells grown in medium with stripped serum and treated with testosterone

378 (100nM) for 0, 30', 60' and 8 hours. Cells were tripsinized and washed with PBS. After
379 centrifugation (5 minutes; 1200rpm), supernatant was discarded, and cells were frozen at -80ºC
380 prior to be sent to the Functional Proteomics Core at MD Anderson.
381
382 **Western blot, immunofluorescence and antibodies**
383 Adherent cells were washed once with PBS and lysed with 8M urea containing 50mM NaCl and
384 50mM Tris-HCl, pH 8.3, 10mM dithiothreitol, 50mM iodoacetamide. Lysates were quantified
385 (Bradford assay), normalized, reduced, and resolved by SDS gel electrophoresis on 4–15%
386 Tris/Glycine gels (Bio-Rad, Hercules, CA, USA). Resolved protein was transferred to PVDF
387 membranes (Millipore, Billerica, MA, USA) using a Semi-Dry Transfer Cell (Bio-Rad), blocked
388 in 5% BSA in TBS-T and probed with primary antibodies recognizing β-actin (Cell Signaling
389 Technology, #3700. Mouse. Lot:14 1:4000, Danvers, MA, USA), ZIP9 (Abcam, #137205,
390 Rabbit mAb. Lot: GR3231323-8. 1:500), P-ERK (Cell Signaling Technology, Phospho-p44/42
391 MAPK (Erk1/2) (Thr202/Tyr204) (D13.14.4E) XP® Rabbit mAb #4370. Lot. 24 1:1000), ERK
392 (Cell Signaling Technology, p44/42 MAPK (Erk1/2) (137F5) Rabbit mAb. Lot: 28 #4695,
393 1:1000), Androgen Receptor [(D6F11) XP® Rabbit mAb #5153. Lot: 7], Recombinant Anti-
394 Androgen Receptor antibody [EPR1535(2)] (ab133273. Antibody already validated by the
395 Human Protein Atlas), RSK1/RSK2/RSK3 [(32D7) Rabbit mAb #9355. Lot:3], Phospho-
396 p90RSK [(Thr359/Ser363)Antibody #9344. Lot: 15]. After incubation with the appropriate
397 secondary antibody [(Rabbit Anti-Mouse IgG H&L (Biotin) preabsoFS9rbed (ab7074); Anti-
398 mouse IgG, HRP-linked Antibody #7076. 1:2000)] proteins were detected using ClarityTM
399 Western ECL Substrate (Bio-Rad. #170-5060). All western blots were repeated at least 3 times.
400 To monitor YAP1 nuclear translocation by western blot analysis, nuclear fractionation was

401 performed using protein lysis buffer containing 10mM HEPES, 1mM KCl, 1.5mM MgCl2 and
402 10% glycerol (Buffer A). After washing the adherent cells with DPBS, samples were
403 resuspended in Buffer A and incubated for 5 minutes on ice in the presence of 0.1% Triton-X-
404 100. After centrifugation, the nuclear fraction remained as a pellet while the supernatant
405 corresponding to the cytosolic fraction. Nuclear fraction was washed with Buffer A. After
406 centrifugation, the nuclear fraction was resuspended in RIPA buffer and samples were boiled for
407 5 min prior to sample loading. The cytosolic fraction was centrifuged for 15 min at 13500 rpm.
408 Only the supernatant was kept after centrifugation. Western blot was performed as described
409 before and the following antibodies were used for protein detection: β-tubulin (Cell Signaling
410 Technology, β-Tubulin (9F3) Rabbit mAb #2128. 1:1000), PARP (Cell Signaling Technology,
411 Rabbit mAb #9542. 1:1000), YAP1 (Cell Signaling Technology, YAP (D8H1X) XP® Rabbit
412 mAb #14074. 1:1000). For immunofluorescence in adherent cells, samples were fixed with 4%
413 paraformaldehyde (Affymetrix; #19943) for 7 min at room temperature and permeabilized with
414 iced-cold methanol. After blocking with 10% FBS:0.03%Triton-X100, primary antibodies were
415 incubated overnight in blocking solution (β-actin and YAP1 antibodies detailed above). After
416 three washes in DPBS:0.03% Triton X-100) cells were incubated with secondary antibodies for
417 45 minutes at room temperature [(Goat anti-Mouse IgG (H+L) Highly Cross-Adsorbed
418 Secondary Antibody, Alexa Fluor 594. Goat anti-Rabbit IgG (H+L) Highly Cross-Adsorbed
419 Secondary Antibody, Alexa Fluor 488)]. Cells were rinsed with PBS-0.03%-Triton three times
420 and coverslips were mounted with ProLong Gold antifade reagent with DAPI (#P36935; Thermo
421 Fisher Scientific). Images were captured using a Leica DM IL microscope and registered using
422 LAS software. For fluorescence intensity quantification ImageJ software (National Institutes of

423 Health, Bethesda, MD, USA) was used, and statistical analyses were performed with GraphPad
424 Prism software.
425
426 **Immunohistochemistry and quantification**
427 FFPE tissue microarrays (ME1004h: Malignant melanoma, metastatic malignant melanoma and
428 nevus tissue array) were obtained from US Biomax, Inc. (Derwood, MD). For the staining with
429 anti-ZIP9 antibody [(SLC39A9 Antibody (PA5-52485), Thermofisher Scientific, Waltham,
430 MA)], slides were deparaffinized and rehydrated following the standard immunohistochemistry
431 protocol [(xylenes 5 minutes x 3, 100% alcohol (5 min. x 3), 95% alcohol (5 min.), 80% alcohol
432 (5 min.), 70% alcohol (5 min.), and 50% alcohol (5 min.) and finished with distilled water)]. The
433 antigen retrieval was done by loading the slides into a retriever (Electron Microscopy Sciences
434 EMS) with R-Buffer A. After 20 minutes, samples were allowed to cool for 30 minutes inside
435 the retriever and for 20 minutes at room temperature. Samples were washed twice with PBS and
436 blocked with Dako Dual Endogenous Enzyme Block (Code S2003. Agilent Santa Clara, CA) for
437 20 minutes at R.T. Samples were washed twice with PBS and blocked for 20 minutes with 2
438 drops of Vector Avidin Block. After washing twice with PBS, slides were blocked for 20
439 minutes with two drops of Vector Biotin Block (Avidin/Biotin Blocking kit. SP-2001. Vector
440 Laboratories, Inc. Burlingame, CA). Samples were washed twice with PBS with Protein Block
441 Serum-Free Ready-To-Use for 30 minutes at R.T. (Code X0909. Agilent Santa Clara, CA).
442 Primary antibody was prepared 1:500 in PBST (100µl per slide) and samples were incubated
443 overnight at 4°C. Samples were washed three times with PBS and incubated with Biotinylated
444 Secondary antibody (Vectastain Kit, Peroxidase Rabbit IgG, PK-4001) for one hour at R.T. After
445 three washes with PBS, ABC reagent (prepared 30 minutes in advance) was added and samples

446 were incubated for 30 minutes at R.T. Samples were washed twice with PBS and incubated for 3
447 minutes with ImmPACT® DAB Substrate, Peroxidase (HRP) (SK-4105. Vector laboratories,
448 Burlingame, CA). Tissues were counterstained with hematoxylin (30 seconds, R.T.) (GHS316.
449 Sigma-Aldrich) dehydrated, and mounted with SecureMount (Fisher HealthCare™
450 PROTOCOL™ Mounting Media. #022-208. Fisher Scientific. Thermofisher Scientific). John T.
451 Seykora M.D., Ph.D, performed scoring of the stained tissue microarray, and scoring index was
452 determined by scoring the percentage of positive cells on a scale of 0 to 3 as well as the intensity
453 of ZIP9 staining on a scale of 0 to 4 (1=1-25%, 2=26-50%, 3=51-75%, 4=76-100%).
454 The staining of the tissue microarrays (ME1004h) for AR detection was performed by
455 University of Pennsylvania Pathology Clinical Service Center—Anatomic Pathology Division,
456 using the highest grade, CLIA (Clinical Laboratory Improvement Amendments) certified and
457 validated test available. Briefly, five-micron sections of formalin-fixed paraffin-embedded tissue
458 were stained using antibody against Androgen Receptor [(Leica AR-318-L-CE, clone AR27
459 (clone AR27, 1:25)]. Staining was done on a Leica Bond-IIITM instrument using the Bond
460 Polymer Refine Detection System (Leica Microsystems DS9800). Heat-induced epitope retrieval
461 was done for 20 minutes with ER2 solution (Leica Microsystems AR9640). All the experiment
462 was done at room temperature. Slides are washed three times between each step with bond wash
463 buffer or water. The slides were reviewed and scored in blinded fashion by a board-certified U.
464 Penn pathologist. Prostate tissue was used as the positive control.
465
466 **Immunocytochemistry**
467 To detect ZIP9 protein in WM46 isogenic clones, the protocol described in ProSciΨ™ for
468 immunocytochemistry. Briefly, cells were fixed in 4% PFA for 7 minutes. After two washes with

469 PBS (5min), cells were permeabilized with PBS/0.1% Triton X-100 for 1 minute at R.T. Cells
470 were washed twice with PBS on a shaker. Once treated with 1.5% H_2O_2/PBS solution for 15
471 minutes (R.T.), cells were washed again and blocked with 5%BSA for one hour at R.T. For
472 primary antibody incubation, α-ZIP9 antibody [(SLC39A9 Antibody (PA5-52485),
473 Thermofisher Scientific, Waltham, MA)] was diluted 1:500 in 1% BSA and cells were incubated
474 overnight at 4ºC. After washing three times with PBS on a shaker, the slide was incubated with
475 Biotinylated Secondary antibody (Vectastain Kit, Peroxidase Rabbit IgG, PK-4001) for one hour
476 at R.T. Cells were washed three times with PBS, ABC reagent (prepared 30 minutes in advance)
477 was added and samples were incubated for 30 minutes at R.T. After three washes with PBS,
478 samples were incubated for 1.5 minutes with Vector Laboratories DAB Peroxidase (HRP)
479 Substrate Kit (NC9276270. Vector laboratories, Burlingame, CA). Cells were counterstain with
480 hematoxylin (10 seconds, R.T.) (GHS316. Sigma-Aldrich) and mounted with SecureMount
481 (Fisher HealthCare™ PROTOCOL™ Mounting Media. #022-208. Fisher Scientific.
482 Thermofisher Scientific).
483
484 **Cell membrane labeling with testosterone-BSA-FITC**
485 WM46 were seeded over coverslips in p12-well culture plate, after 24 hours cells TU2% media
486 was removed, and cells were grown in Serum-free TU media for 24 hours. Cells were treated
487 with APA (8mM) or DMSO as vehicle control. After one hour, cells were treated with 0.25μM
488 testosterone 3-(O-carboxymethyl) oxime:BSA-fluorescein isothiocyanate (T-BSA-FITC)
489 conjugate (T5771, Sigma-Aldrich, Munich, Germany) diluted in Tris-Buffer (pH 7.2) for 20 min
490 at room temperature. Negative control cells were incubated with 0.25 μM BSA-FITC (A9771,
491 Sigma-Aldrich, Munich, Germany) diluted in Tris-Buffer (pH 7.2) for 20 min at room

492 temperature. The medium was then aspirated, and cells were fixed for 7 minutes with 4%PFA.
493 Cells were washed three times with PBS (5 minutes each) and mounted with ProLong Gold
494 antifade reagent with DAPI (#P36935; Thermo Fisher Scientific). Images were captured using a
495 Leica DM IL microscope and registered using LAS software.
496
497 **Quantitative RT-PCR**
498 RNA was extracted using RNeasy kit (Qiagen. #74104) following the manufacturer's
499 instructions. cDNA was obtained using High Capacity cDNA Reverse Transcription Kit
500 (Applied Biosystems #4368814). For quantitative real-time PCR, PowerUP™ SYBR™ Green
501 Master Mix (Applied Biosystems #A25741) was used. ViiA 7 Real-Time PCR System was used
502 to perform the reaction (Applied Biosystems). Values were corrected by β-actin expression. The
503 $2^{-\Delta\Delta Ct}$ method was applied to calculate the relative gene expression. Primers used for the
504 amplification are included in Table S2.
505
506 **Mice, subcutaneous tumors and pharmacologic treatments**
507 All mice were purchased from Taconic Biosciences, Inc. (Rensselaer, NY, USA). 8- to 10-week
508 old male and female C57BL/6NTac or IcrTac:ICR-Prkdcscid mice were allowed to reach
509 sexually mature ages or to acclimatize for one week prior to being used in experiments. These
510 studies were performed without inclusion/exclusion criteria or blinding but included
511 randomization. Based on a two-fold anticipated effect, we performed experiments with at least 5
512 biological replicates. All procedures were performed in accordance with International Animal
513 Care and Use Committee (IACUC)-approved protocols at the University of Pennsylvania.
514 Subcutaneous tumors were initiated by injecting tumor cells in 50% Matrigel (Corning, Bedford,

515 MA, USA) into the subcutaneous space on the right flanks of mice. 10 x 10^6 human WM46 or 10
516 x 10^5 murine YUMM1.7 cells were used for each tumor. Oral administration of vehicle,
517 bicalutamide (30mg/kg/day) or apalutamide (20mg/kg/day) was performed daily. 100µl of drug
518 was administrated by oral gavage [10%DMSO:90%Vehicle (15% ethanol:85% sesame oil)].
519 Each experiment include n=5 replicates, which provide 100% power to detect at least a 50%
520 difference between groups with 95% confidence. The size of each animal cohort was determined
521 by estimating biologically relevant effect sizes between control and treated groups and then
522 using the minimum number of animals that could reveal statistical significance using the
523 indicated tests of significance. When in vivo experiments were performed with female, mice
524 located in different cages, animals were randomized prior to cell inoculation or drug treatment.
525 All animals housed within the same cage were placed within the same treatment group. Weight
526 and health status of the mice as well as tumor growth were monitored daily. As subcutaneous
527 tumors grew in mice, perpendicular tumor diameters were measured using calipers. Volume was
528 calculated using the formula $L \times W^2 \times 0.52$, where L is the longest dimension and W is the
529 perpendicular dimension. Animals were euthanized when tumors exceeded a protocol-specified
530 size of 15 mm in the longest dimension. Secondary endpoints include severe ulceration, death,
531 and any other condition that falls within the IACUC guidelines for Rodent Tumor and Cancer
532 Models at the University of Pennsylvania.
533
534 **Statistical analysis**
535 For experiments comparing two groups (treated vs control), significance was calculated using the
536 Mann-Whitney test. For experiments with more than two groups, one-way ANOVA with
537 Tukey's honest significance difference test was performed. For the tumor growth studies *in vivo*,

538 non-linear regression analysis was performed to get the Exponential Growth Equation and
539 doubling times for tumor growth. To analyze the slopes of the curves and to compare them
540 between groups, linear regression analysis was performed. All the statistical analyses in this
541 work were performed using Graphpad Prism Software. Error bars represent standard error of the
542 mean (SEM). **** p value≤0.0001; *** p value≤0.001; ** p value≤0.01; * p value≤0.05;
543 n.s>0.05.
544

545 **Acknowledgements**
546 The authors thank the University of Pennsylvania Skin Biology and Disease Research-based
547 center for analysis of tissue sections and University of Pennsylvania Pathology Clinical Service
548 Center—Anatomic Pathology Division for the AR staining of the tissue microarray. **Funding:**
549 T.W.R. is supported by grant from the NIH/NCI (R01 CA163566, R41CA228695), and by the
550 Stiefel award from the Dermatology Foundation. This work was also supported in part by the
551 Penn Skin Biology and Diseases Resource-based Center (P30-AR069589), the Melanoma
552 Research Foundation to T.W.R., and R37 GM56328 to J.K.F**.**
553

554 **Author Contributions**
555 C.A.P., R.P., A.T. performed the experiments. C.A.P., R.P. and J.K.F designed and performed
556 the experiments to study zinc influx. J.K.F provided experimental material and reviewed the
557 manuscript. J.T.S, scored the tissue microarray and reviewed the manuscript. C.A.P, C.A.N. and
558 T.W.R designed experiments and wrote the article. Competing interests: C.A.P., C.A.N., and
559 T.W.R., and are inventors on a provisional patent held by the University of Pennsylvania related
560 to this work.

561 **References**

562

563 1. Siegel, R. L., Miller, K. D. & Jemal, A. Cancer statistics, 2020. *CA Cancer J Clin* **70**, 7–
564 30 (2020).
565 2. GLOBOCAN2018. https://bit.ly/2Vd3C6a.
566 3. Clemmesen, J. & Busk, T. Cancer Mortality Among Males and Females in Denmark,
567 England, and Switzerland: V. Incidence of Accessible and Inaccessible Cancers in Danish Towns
568 and Rural Areas. *Cancer Res* **9**, 415–421 (1949).
569 4. Hieken, T. J. *et al.* Sex-Based Differences in Melanoma Survival in a Contemporary
570 Patient Cohort. *Journal of Women's Health* (2020) doi:10.1089/jwh.2019.7851.
571 5. GLOBOCAN2018. Sex disparities in melanoma survival over time. shorturl.at/bkAI6.
572 6. Natale, C. A. *et al.* Activation of G protein-coupled estrogen receptor signaling inhibits
573 melanoma and improves response to immune checkpoint blockade. *Elife* **7**, (2018).
574 7. Natale, C. A. *et al.* Sex steroids regulate skin pigmentation through nonclassical
575 membrane-bound receptors. *Elife* **5**, (2016).
576 8. Sperling, M. A. *Pediatric Endocrinology-Mean Sex Steriod Concentration in Infants,*
577 *Children and adults.* (Elsevier Health Sciences, 2014).
578 9. Watts, E. L. *et al.* Prospective analyses of testosterone and sex hormone-binding globulin
579 with the risk of 19 types of cancer in men and postmenopausal women in UK Biobank. *Int J*
580 *Cancer* (2021) doi:10.1002/ijc.33555.
581 10. Barbosa-Desongles, A., Hernández, C., Simó, R. & Selva, D. M. Testosterone induces
582 cell proliferation and cell cycle gene overexpression in human visceral preadipocytes. *Am. J.*
583 *Physiol., Cell Physiol.* **305**, C355-359 (2013).
584 11. Fu, R. *et al.* Novel evidence that testosterone promotes cell proliferation and
585 differentiation via G protein-coupled receptors in the rat L6 skeletal muscle myoblast cell line. *J.*
586 *Cell. Physiol.* **227**, 98–107 (2012).
587 12. Rodríguez-Lozano, D. C., Piña-Medina, A. G., Hansberg-Pastor, V., Bello-Alvarez, C. &
588 Camacho-Arroyo, I. Testosterone Promotes Glioblastoma Cell Proliferation, Migration, and
589 Invasion Through Androgen Receptor Activation. *Front. Endocrinol.* **10**, (2019).
590 13. Maasberg, M. *et al.* Androgen receptors, androgen-dependent proliferation, and 5 alpha-
591 reductase activity of small-cell lung cancer cell lines. *Int. J. Cancer* **43**, 685–691 (1989).
592 14. Allil, P. A. A., Visconti, M. A. & Isoldi, A. M. L. C. and M. C. Photoperiod and
593 Testosterone Modulate Growth and Melanogenesis of S91 Murine Melanoma. *Medicinal*
594 *Chemistry* http://www.eurekaselect.com/82341/article (2008).
595 15. Ma, M. *et al.* Sustained androgen receptor signaling is a determinant of melanoma cell
596 growth potential and tumorigenesis. *J Exp Med* **218**, (2021).
597 16. Meeth, K., Wang, J. X., Micevic, G., Damsky, W. & Bosenberg, M. W. The YUMM
598 lines: a series of congenic mouse melanoma cell lines with defined genetic alterations. *Pigment*
599 *Cell Melanoma Res* **29**, 590–597 (2016).
600 17. Gao, W., Bohl, C. E. & Dalton, J. T. Chemistry and Structural Biology of Androgen
601 Receptor. *Chem Rev* **105**, 3352–3370 (2005).
602 18. Askew, E. B., Gampe, R. T., Stanley, T. B., Faggart, J. L. & Wilson, E. M. Modulation of
603 Androgen Receptor Activation Function 2 by Testosterone and Dihydrotestosterone. *J. Biol.*
604 *Chem.* **282**, 25801–25816 (2007).
605 19. Berg, A. H., Rice, C. D., Rahman, M. S., Dong, J. & Thomas, P. Identification and
606 characterization of membrane androgen receptors in the ZIP9 zinc transporter subfamily: I.

607 Discovery in female atlantic croaker and evidence ZIP9 mediates testosterone-induced apoptosis
608 of ovarian follicle cells. *Endocrinology* **155**, 4237–4249 (2014).
609 20. Matsuura, W. *et al.* SLC39A9 (ZIP9) regulates zinc homeostasis in the secretory
610 pathway: characterization of the ZIP subfamily I protein in vertebrate cells. *Biosci. Biotechnol.*
611 *Biochem.* **73**, 1142–1148 (2009).
612 21. Fatfat, M. *et al.* Copper chelation selectively kills colon cancer cells through redox
613 cycling and generation of reactive oxygen species. *BMC Cancer* **14**, 527 (2014).
614 22. He, L. *et al.* ZIP8, member of the solute-carrier-39 (SLC39) metal-transporter family:
615 characterization of transporter properties. *Mol. Pharmacol.* **70**, 171–180 (2006).
616 23. Zhang, L. *et al.* OSskcm: an online survival analysis webserver for skin cutaneous
617 melanoma based on 1085 transcriptomic profiles. *Cancer Cell Int* **20**, 176 (2020).
618 24. Leal, M. F. *et al.* Clinical implication of 14-3-3 epsilon expression in gastric cancer.
619 *World J. Gastroenterol.* **18**, 1531–1537 (2012).
620 25. Ruas, M. & Peters, G. The p16INK4a/CDKN2A tumor suppressor and its relatives.
621 *Biochim. Biophys. Acta* **1378**, F115-177 (1998).
622 26. Germann, U. A. *et al.* Targeting the MAPK Signaling Pathway in Cancer: Promising
623 Preclinical Activity with the Novel Selective ERK1/2 Inhibitor BVD-523 (Ulixertinib). *Mol.*
624 *Cancer Ther.* **16**, 2351–2363 (2017).
625 27. Han, Y. Analysis of the role of the Hippo pathway in cancer. *Journal of Translational*
626 *Medicine* **17**, 116 (2019).
627 28. Zhao, B., Li, L., Tumaneng, K., Wang, C.-Y. & Guan, K.-L. A coordinated
628 phosphorylation by Lats and CK1 regulates YAP stability through SCFβ-TRCP. *Genes Dev* **24**,
629 72–85 (2010).
630 29. Fujii, M. Exploration of a new drug that targets YAP. *J. Biochem.* **152**, 209–211 (2012).
631 30. Bulldan, A., Malviya, V. N., Upmanyu, N., Konrad, L. & Scheiner-Bobis, G.
632 Testosterone/bicalutamide antagonism at the predicted extracellular androgen binding site of
633 ZIP9. *Biochim Biophys Acta Mol Cell Res* **1864**, 2402–2414 (2017).
634 31. Ponnusamy, S. *et al.* Orally-Bioavailable Androgen Receptor Degrader, A Potential
635 Next-Generation Therapeutic for Enzalutamide-Resistant Prostate Cancer. *Clin. Cancer Res.*
636 (2019) doi:10.1158/1078-0432.CCR-19-1458.
637 32. Chi, K. N. *et al.* Apalutamide for Metastatic, Castration-Sensitive Prostate Cancer. *N.*
638 *Engl. J. Med.* **381**, 13–24 (2019).
639 33. Kayigil, O., Atahan, O. & Metin, A. Cyproterone acetate monotherapy in advanced
640 prostatic carcinoma. *Int Urol Nephrol* **29**, 213–220 (1997).
641 34. Fukada, T. & Kambe, T. Molecular and genetic features of zinc transporters in
642 physiology and pathogenesis. *Metallomics* **3**, 662–674 (2011).
643 35. Costello, L. C., Liu, Y., Zou, J. & Franklin, R. B. Evidence for a zinc uptake transporter
644 in human prostate cancer cells which is regulated by prolactin and testosterone. *J Biol Chem* **274**,
645 17499–17504 (1999).
646 36. Bafaro, E., Liu, Y., Xu, Y. & Dempski, R. E. The emerging role of zinc transporters in
647 cellular homeostasis and cancer. *Signal Transduction and Targeted Therapy* **2**, 1–12 (2017).
648 37. Klein, S. L. & Flanagan, K. L. Sex differences in immune responses. *Nat. Rev. Immunol.*
649 **16**, 626–638 (2016).
650

651

652 **Figure legends**

653 **Fig. 1: Biologic sex and testosterone promote proliferation of melanoma models lacking**
654 **detectable AR. A.** Tumor growth of human WM46 melanoma in male and female
655 immunodeficient SCID mice. Tumor doubling times are 16.2 and 18.6 days for males and
656 females respectively (Non-linear regression analysis/Exponential fit. See also Sup. Fig. 1 for
657 expanded statistical analysis). **B.** Cell proliferation (cell number) determined after 6 days of
658 treatment with vehicle (DMSO), 100nM testosterone (T) or 100nM dihydrotestosterone (DHT).
659 Human primary melanocytes (H.Mel.) and human melanoma WM46 cells are shown. Graphs
660 represent the average of three independent experiments. **C.** Cell proliferation of human WM46
661 and murine YUMM1.7 melanoma cells exposed to increasing concentrations of testosterone (T)
662 (left panels) or dihydrotestosterone (DHT) (right panel). **D.** AR protein expression determined by
663 Western blot with two different antibodies. Upper line = Androgen Receptor [(D6F11) XP®
664 Rabbit mAb #5153. Lower line = Recombinant Anti-Androgen Receptor antibody [EPR1535(2)]
665 (ab133273). The prostate cancer cell line DU 145 was used as a postivie control.). β-actin was
666 used as loading control. A replicate with increased exposure time is shown in Fig. S1G. **E.**
667 RNA-seq data from 6 different primary melanocyte cell lines reported as median FPKM (number
668 Fragments Per Kilobase of exon per Million reads). Melanocytic Receptor 1 (MC1R) and
669 Glucocorticoid Receptor (NR3C1) were used as positive controls for membrane and nuclear
670 receptors respectively.

671 ** p value≤0.01; * p value≤0.05.

672

673 **Fig 2: ZIP9 is active in human melanoma cells, and is broadly expressed in human**
674 **melanocytic tumors. A.** ZIP9 protein expression determined by western blot in primary
675 melanocytes and a battery of human melanoma cell lines. **B.** Time-lapse *in vivo* analysis of Zn^{++}

676 influx in WM46 cells upon testosterone addition (100nM). FluoZin-3 was used as Zn^{++} reporter.
677 **C.** Intracellular levels of Zn^{++} after long-term testosterone treatment (96 hours; 100nM
678 testosterone). Zinc levels were measured as fluorescence intensity per cell. FluoZin-3 was used
679 as Zn^{++} reporter. Representative images are shown on the right at indicated time-points. **D.**
680 WM46 relative proliferation (cell number) after 6 days in the presence of 100 nM testosterone
681 (T) +/- 200 nM zinc chelator (TPEN). **E.** WM46 proliferation in the presence exogenous divalent
682 cations Zn^{++} Fe^{++} and Mn^{++}. Cells were grown for 6 days and treated as indicated in the legend.
683 Error bars represent standard error of the mean (SEM). **F.** Validation of ZIP9 [(SLC39A9
684 Antibody (PA5-52485)] and androgen receptor [(Leica AR-318-L-CE, clone AR27 (clone AR27,
685 1:25)] antibodies for immunohistochemistry. ZIP9 staining performed in wild-type and ZIP9
686 knock-out cells. Non permeabilization of the cells ensured ZIP9 membrane localization. Prostate
687 gland tissue and human prostate cancer samples were used as positive controls for AR.
688 Representative images of human melanoma samples stained for ZIP9 and AR. Tumors
689 expressing low, medium and high levels of ZIP9 are shown. Replicates from the same samples
690 stained for AR are shown. 20X magnification (1.6X zoom). Scale bar=60μM. **G.** Graphic
691 representation of the % of tumors that express ZIP9. Data from nevus, primary melanomas and
692 metastatic melanoma are displayed. **H.** Graphic representation of the percentage of nevi, primary
693 lesions and metastatic tumors classified according to ZIP9 intensity (Score 1=1-25%, 2=26-50%,
694 3=51-75%, 4=76-100%).
695 **** p value≤0.0001; ** p value≤0.01; * p value≤0.05; n.s>0.05.
696
697 **Fig. 3: ZIP9 mediates testosterone effects in melanoma. A.** Proliferation (cell number) of
698 isogenic clonal populations of WM46 wtZIP9 and ΔZIP9 (gRNA #3) cells exposed to increasing
699 concentrations of testosterone (T) and dihydrotestosterone (DHT). **B.** Proliferation (cell number)

700 of isogenic clonal populations of WM46 wtZIP9 and ΔZIP9 (gRNA #4) cells exposed to
701 increasing concentrations of testosterone (T) and dihydrotestosterone (DHT). The graph
702 represents the average of three independent experiments. **C.** Intracellular levels of zinc in human
703 melanoma ΔZIP9 cells measured as relative fluorescence intensity of FluoZin-3. Graphs
704 represent the average of three independent experiments. **D.** Relative cell proliferation in the
705 presence of 100nM testosterone (T), zinc chelator (200nM TPEN) and $ZnCl_2$ (400nM). Cells
706 were cultured for 6 days. The graph represents the average of three independent experiments.
707 **** p value≤0.0001; ** p value≤0.01; * p value≤0.05; n.s>0.05.
708
709 **Fig. 4: Testosterone driven increase in melanoma proliferation requires ZIP9 and**
710 **activation of MAPK and YAP1. A.** RPPA analysis displaying changes in protein expression in
711 WM46 human melanoma cells following exposure to 100 nM testosterone (T) for increasing
712 amounts of time. Down-regulated proteins are shown in black; white color corresponds to up-
713 regulated proteins and control proteins showing no fold-change when compared to vehicle-
714 treated cells are shown in dark grey. **B.** Relative proliferation (cell number) after exposure to
715 pharmacologic ERK1/2 inhibition via 50nM RVD-523 (Ei) alone or in combination with
716 testosterone. wtZIP9 and ΔZIP9 WM46 cells are shown. The western blot shows levels of
717 phosphorylation of the ERK target RSK in wtZIP9 and ΔZIP9 WM46 cells (Ei represents RVD-
718 523). **C.** Western blot for YAP1 in fractionated WM46 lysates. Cells were treated with 100 nM
719 testosterone for the indicated times. β-Actin is used as cytoplasmic fraction positive control.
720 PARP is used as nuclear fraction positive control. **D.** Quantification of YAP-1 nuclear
721 immunodetection after 30 minutes of exposure to 100 nM testosterone (T) and/or 8μM
722 dobutamine (Dob) in wtZIP9 and ΔZIP9 cells. **E.** Proliferation of wtZIP9 and ΔZIP9 WM46

723 cells after treatment with 100nM testosterone (T) and/or the YAP inhibitor dobutamine (Dob). **F.**
724 Relative mRNA expression of YAP1 target genes after 30 minutes in the presence of 100 nM
725 testosterone and/or 8μM dobutamine. Error bars represent standard error of the mean (SEM).
726 *** p value≤0.001; ** p value≤0.01; * p value≤0.05; n.s>0.05.
727
728 **Fig. 5: Pharmacologic ZIP9 blockade inhibits melanoma *in vivo*. A.** Proliferation of human
729 melanoma cells (WM46) in the presence of 100 nM testosterone (T) +/- 2 μM AR inhibitors
730 (BIC:Bicalutamide; ENZ:Enzalutamide; APA:Apalutamide). Western blot showing ERK and p-
731 ERK proteins in WM46 cells treated with 100nM testosterone +/- 2μM BIC +/- 200 nM zinc
732 chelator (TPEN). **B.** Cell proliferation in human and murine derived melanoma cells [SK-MEL-3
733 (male), SK-MEL-2 (female) and YUMM1.7(male)] treated with 100 nM testosterone (T) in
734 combination with apalutamide (2 μM) (APA). **C.** Cell membrane labeling with cell impermeable
735 testosterone-BSA conjugated with FITC (0.25 μM). BSA-FITC (0.25 μM) was used as a
736 negative control for unspecific binding. Quantification of membrane labeling with T-BSA or the
737 control BSA. The graph represents the fluorescence intensity relative to the total area of each
738 cell. **D.** Proliferation of WM46 wtZIP9 and ΔZIP9 treated with 100 nM testosterone (T) in
739 combination with apalutamide (2 μM) (APA). **E.** Tumor growth and survival analysis in SCID
740 male mice bearing WM46 derived subcutaneous tumors (APA treatment: 20 mg/kg/day via oral
741 gavage). ** p-value<0.005 by ANOVA. Doubling time (non-linear regression analysis):
742 Vehicle=11.11 days; APA=25.22 days. **F.** Tumor growth in mice bearing WM46 derived
743 subcutaneous tumors. Daily treatment with bicalutamide (30 mg/kg/day, via oral gavage) or
744 vehicle are shown for both male and female mice. Linear regression analysis of slopes
745 demonstrates significant differences between vehicle treated and Bic treated males (p-

746 value<0.0001) (See Fig. S6B and S6C). **G.** Tumor growth in SCID male mice bearing ΔZIP9
747 WM46 melanoma. Mice were treated daily with bicalutamide (30 mg/kg/day) or vehicle via oral
748 gavage. . See also Sup. Fig. 6 for expanded statistical analysis).
749 **** p value≤0.0001; *** p value≤0.001; ** p value≤0.01; * p value≤0.05; n.s>0.05.
750
751 **Fig. 6: Working model.** ZIP9 activation promotes ERK phosphorylation and induces YAP1
752 nuclear translocation. AR inhibitors [represented in the figure by apalutamide (APA)] block
753 testosterone effects through ZIP9 inactivation.
754
755
756
757
758
759
760
761
762
763
764
765
766
767
768

769 **Figures**

Figure 1

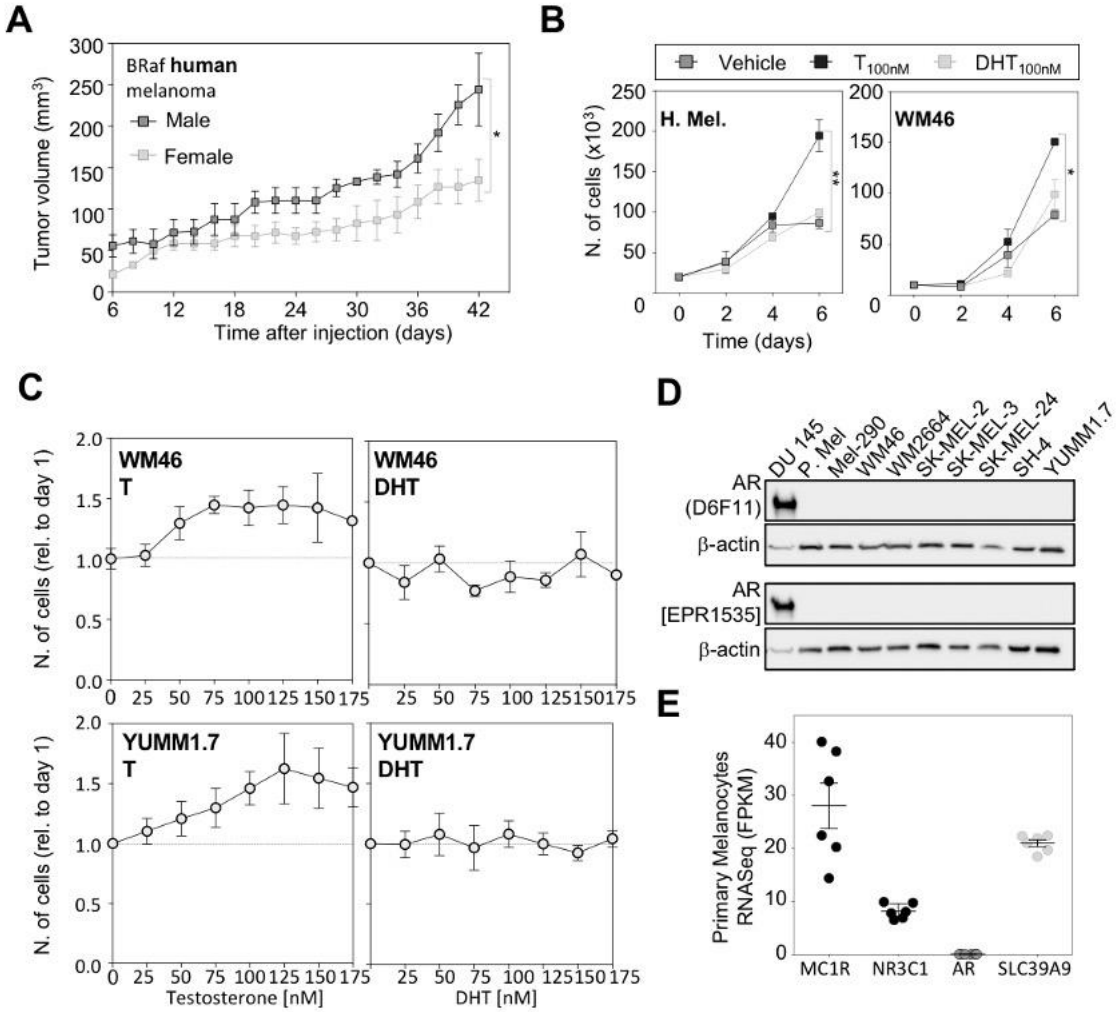

770

Figure 2

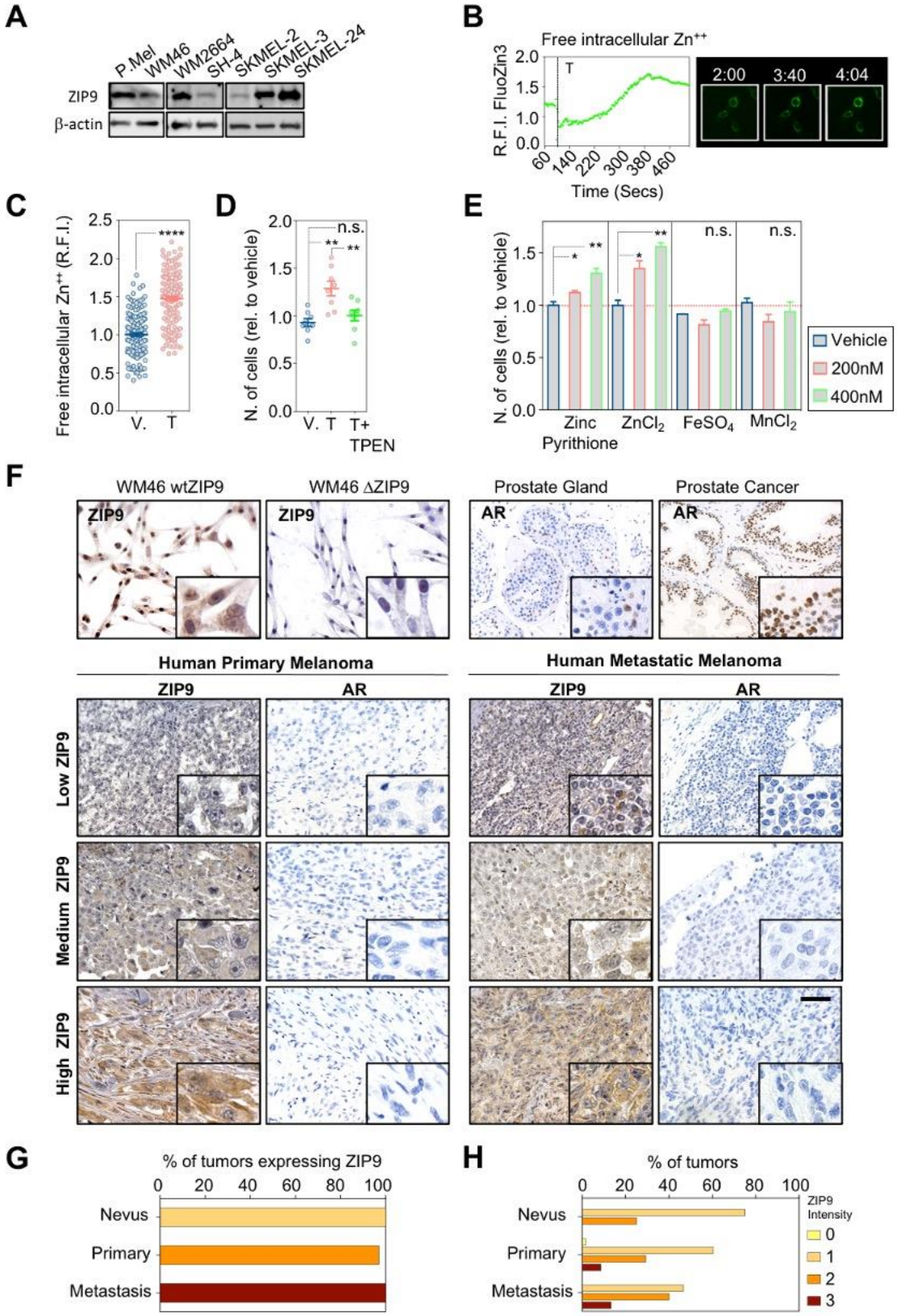
A
P.Mel
WM46
WM2664
SH-4
SKMEL-2
SKMEL-3
SKMEL-24
ZIP9
β-actin
B
Free intracellular Zn++
R.F.I. FluoZin3
T
2:00
3:40
4:04
Time (Secs)
C
Free intracellular Zn++ (R.F.I.)
****
V.
T
D
N. of cells (rel. to vehicle)
n.s.
**
V.
T
T+ TPEN
E
N. of cells (rel. to vehicle)
Zinc Pyrithione
ZnCl2
FeSO4
MnCl2
Vehicle
200nM
400nM
F
WM46 wtZIP9
WM46 ΔZIP9
Prostate Gland
Prostate Cancer
ZIP9
AR
Human Primary Melanoma
Human Metastatic Melanoma
Low ZIP9
Medium ZIP9
High ZIP9
G
% of tumors expressing ZIP9
Nevus
Primary
Metastasis
H
% of tumors
ZIP9 Intensity
0
1
2
3

771

Figure 3

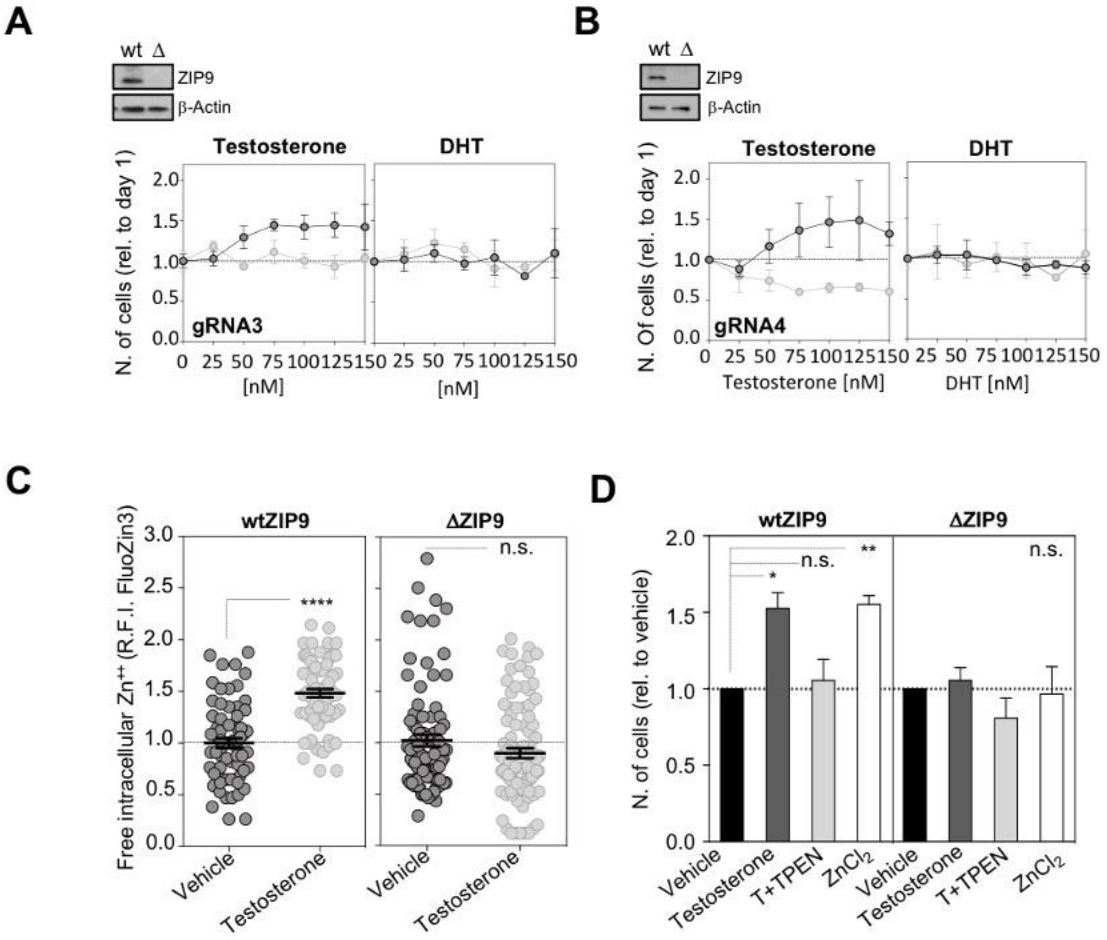

772

773
774
775
776

Figure 4

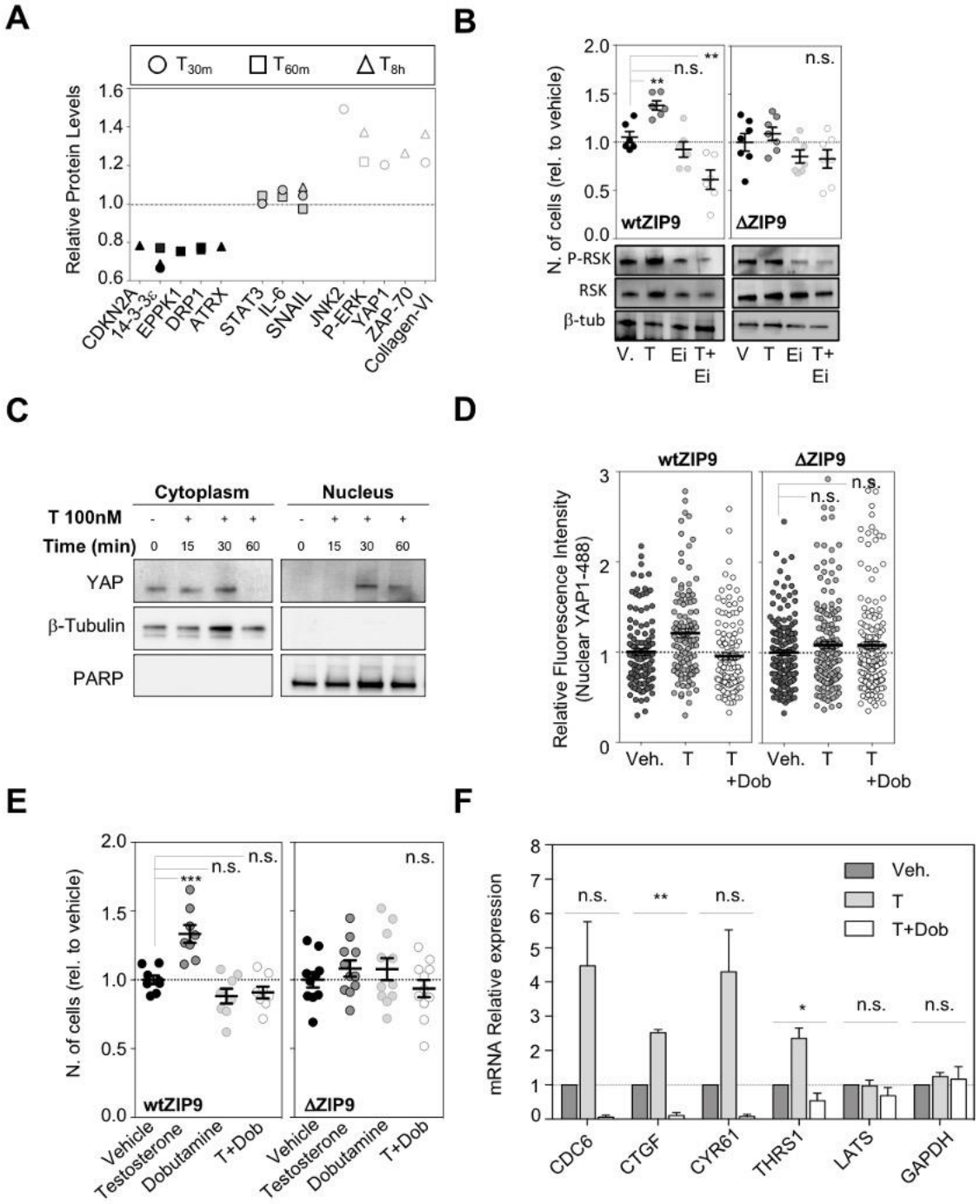

777
778

Figure 5

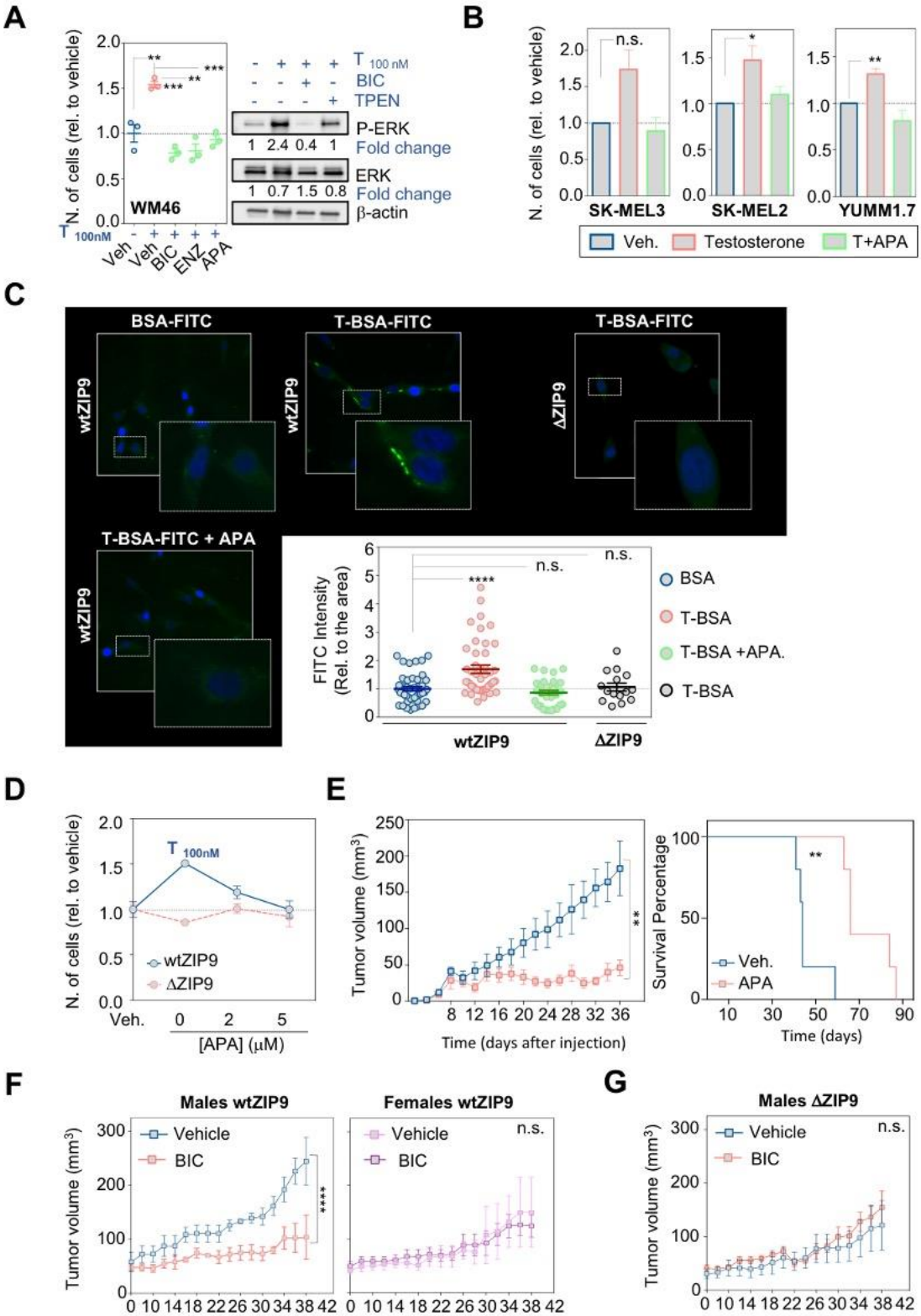
A
N. of cells (rel. to vehicle)
WM46
T 100nM
Veh
Veh
BIC
ENZ
APA
T 100 nM
BIC
TPEN
P-ERK
1 2.4 0.4 1
Fold change
ERK
1 0.7 1.5 0.8
Fold change
β-actin
B
N. of cells (rel. to vehicle)
n.s.
SK-MEL3
SK-MEL2
YUMM1.7
Veh.
Testosterone
T+APA
C
BSA-FITC
T-BSA-FITC
T-BSA-FITC
T-BSA-FITC + APA
wtZIP9
ΔZIP9
FITC Intensity (Rel. to the area)
n.s.
BSA
T-BSA
T-BSA +APA.
T-BSA
wtZIP9
ΔZIP9
D
N. of cells (rel. to vehicle)
T 100nM
wtZIP9
ΔZIP9
Veh.
[APA] (μM)
E
Tumor volume (mm³)
Time (days after injection)
Survival Percentage
Veh.
APA
Time (days)
F
Males wtZIP9
Females wtZIP9
Vehicle
BIC
n.s.
Tumor volume (mm³)
G
Males ΔZIP9
Vehicle
BIC
n.s.
Tumor volume (mm³)

779

Figure 6

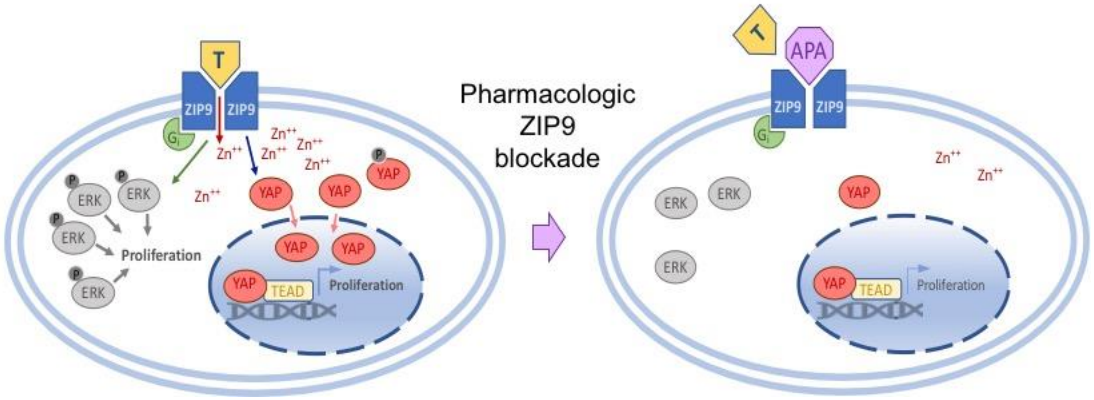
T
ZIP9
ZIP9
Gq
Zn++
Zn++
Zn++
Zn++
Zn++
ERK
ERK
ERK
ERK
Proliferation
YAP
YAP
YAP
YAP
YAP
YAP
TEAD
Proliferation
Pharmacologic
ZIP9
blockade
T
APA
ZIP9
ZIP9
Gq
Zn++
Zn++
ERK
ERK
ERK
YAP
YAP
TEAD
Proliferation

811 **Supplementary Figures**

Supplementary Figure 1

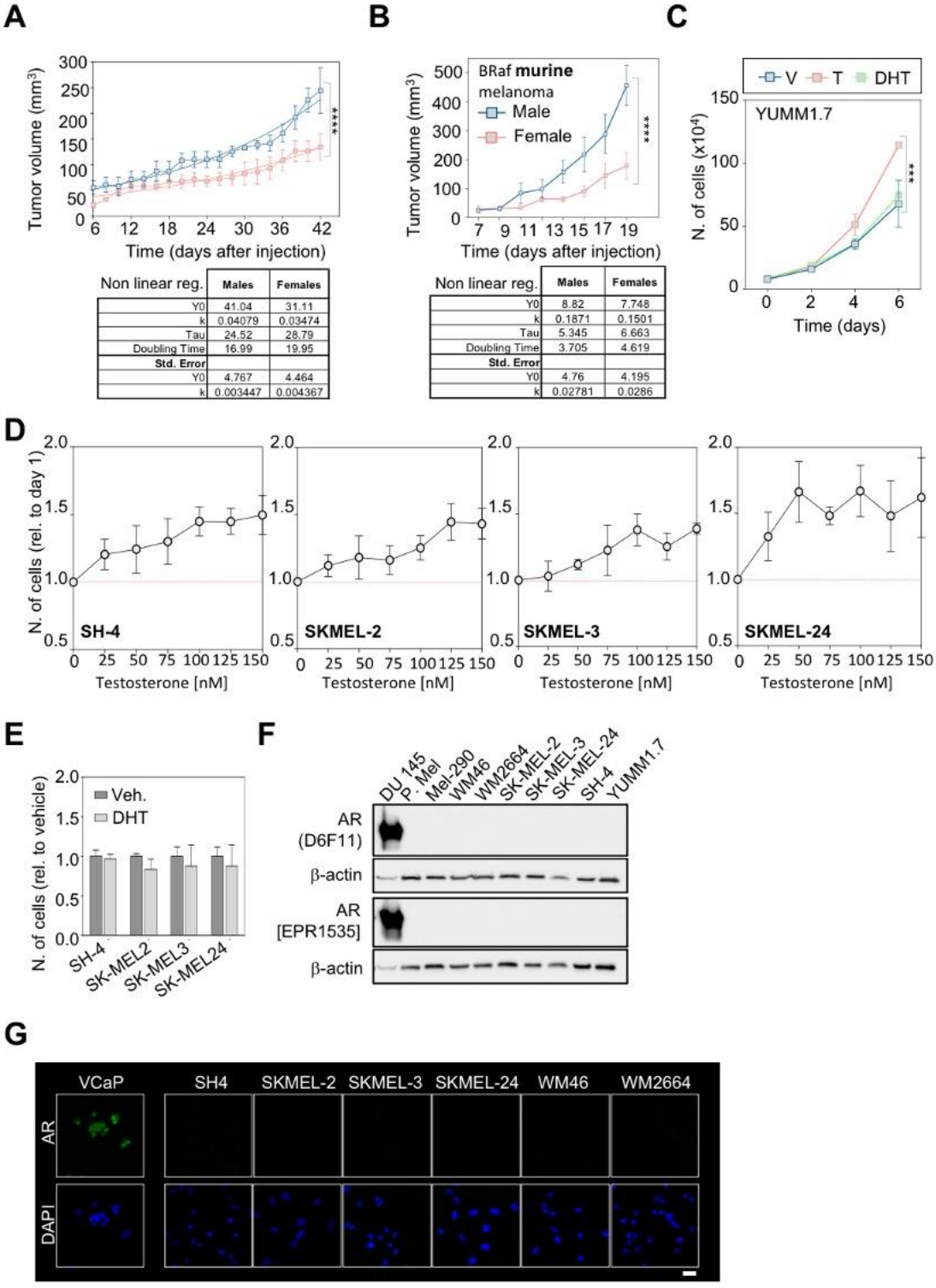

Non linear reg.	Males	Females
Y0	41.04	31.11
k	0.04079	0.03474
Tau	24.52	28.79
Doubling Time	16.99	19.95
Std. Error		
Y0	4.767	4.464
k	0.003447	0.004367

Non linear reg.	Males	Females
Y0	8.82	7.748
k	0.1871	0.1501
Tau	5.345	6.663
Doubling Time	3.705	4.619
Std. Error		
Y0	4.76	4.195
k	0.02781	0.0286

812 **Fig. S1.** Non-linear regression analysis (Exponential fit) for males and females. Doubling time
813 for tumor growth: males=16.99 days and females=19.95 days. (Linear-regression analysis for
814 slope comparison: **** p-value<0.0001). **B.** Tumor growth in C57BL/6 male and female mice
815 bearing syngeneic murine melanoma (YUMM1.7). Doubling time for tumor growth: males = 3.7
816 days, females = 4.6 days (Linear-regression analysis for slope comparison: **** p-
817 value<0.0001). **C.** YUMM1.7 cell number determined after 6 days of treatment with vehicle
818 (DMSO), 100 nM testosterone (T) or 100 nM dihydrotestosterone (DHT). Graphs represent the
819 average of three independent experiments. Error bars represent standard error of the mean
820 (SEM). **D.** Relative cell proliferation of human melanoma cell lines treated for 6 days with
821 increasing concentrations of testosterone (T). **E.** Relative cell proliferation of human melanoma
822 cells treated for 6 days with dihydrotestosterone (DHT 100 nM). **F.** Immunofluorescence
823 detecting AR (D6F11) in a battery of human-derived melanoma cells. AR is shown in green;
824 DNA was stained with DAPI and it is shown in blue. Scale bar 25μM. Error bars represent
825 standard error of the mean (SEM). **G.** AR protein expression determined by Western blot in
826 Melanoma cells. Replicate from Fig. 1D to show higher exposure times for the AR.
827 *** p value≤0.001; **** p value≤0.0001.
828 .
829
830
831
832
833
834
835

Supplementary Figure 2

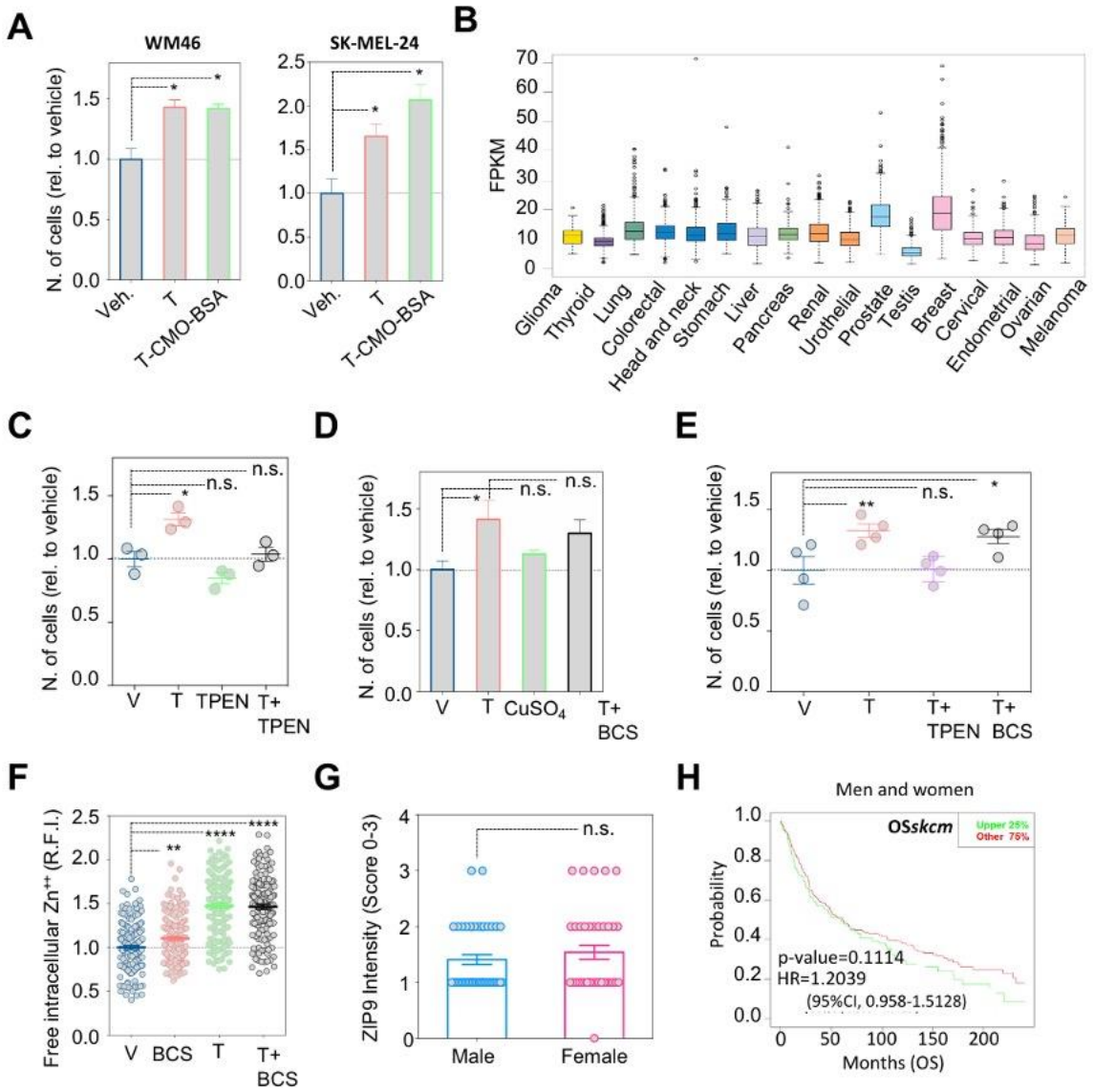

Fig. S2. A. Cell proliferation in human derived melanoma cells [WM46 (female), SK-MEL-24 (male)] treated for 8 days with 100 nM testosterone (T) and the non-permeable analogue Testosterone-CMO-BSA. **B.** RNA-seq data from 17 cancer types reported as median FPKM (number Fragments Per Kilobase of exon per Million reads), generated by the The Cancer Genome Atlas (TCGA). RNA cancer tissue category calculated based on mRNA expression

842 levels across all 17 cancer tissues and include: cancer tissue enriched, cancer group enriched,
843 cancer tissue enhanced, expressed in all, mixed and not detected. Normal distribution across the
844 dataset is visualized with box plots, shown as median and 25th and 75th percentiles. Points are
845 displayed as if they are above or below 1.5 times the interquartile range. **C.** WM46 relative
846 proliferation (cell number) in presence of 100 nM testosterone (T) +/- 200 nM zinc chelator
847 TPEN. **D.** WM46 proliferation treated with 100 nM testosterone (T), +/- copper sulfate
848 (CuSO4) and copper chelator (25μM BCS). **E.** Relative cell proliferation of WM46 cells treated
849 with testosterone (100nM) +/- zinc chelator TPEN (200nM) and the copper chelator BCS
850 (25μM). **F.** Relative intracellular Zn^{++} in cells treated with testosterone and/or copper chelator
851 (BCS). The graph represents relative fluorescence intensity. Error bars represent standard error
852 of the mean (SEM). **G.** Graphic representation of ZIP9 staining intensity in human samples from
853 nevus, primary melanoma and metastatic melanoma in males vs. females (Score 1=1-25%, 2=26-
854 50%, 3=51-75%, 4=76-100%). n.s>0.05. **H.** Overall survival analysis from men and women
855 diagnosed with skin cutaneous melanoma. Data extracted from the following datasets:
856 (GSE17275, GSE19234, GSE22155_GPL6102, GSE22155_GPL6947, GSE50509, GSE46517,
857 GSE53118, GSE65904, GSE98394 and TCGA (1085 tumors; 563 death events). Graphic
858 representation was modified from *OSskcm*. The Kaplan–Meier (KM) survival curves, Hazard
859 ratio (HR) and 95% confidence interval (95%CI) were calculated in a univariate Cox regression
860 analysis.
861 **** p value≤0.0001; ** p value≤0.01; * p value≤0.05; n.s>0.05.
862
863
864

Supplementary Figure 3

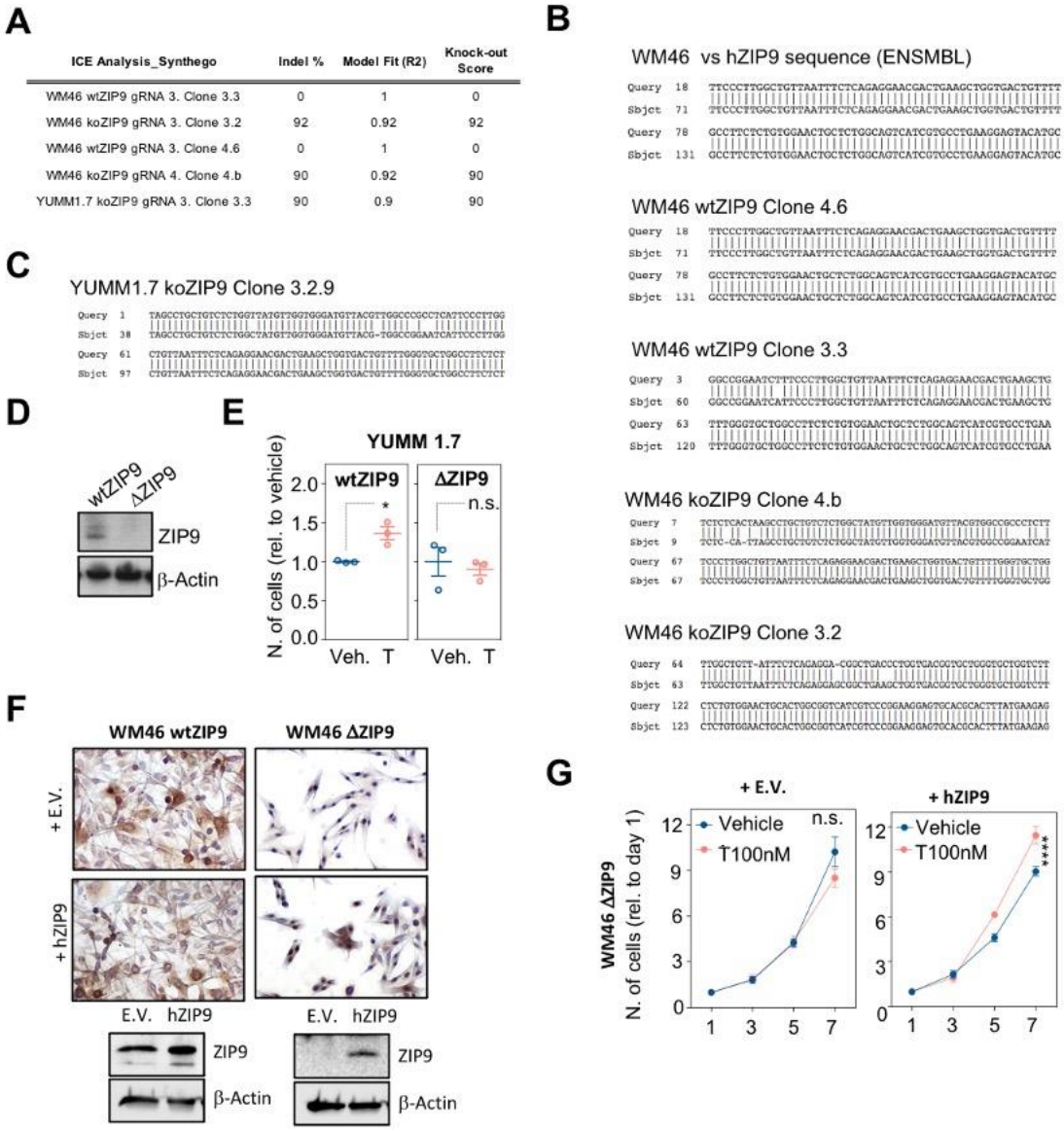

ICE Analysis_Synthego	Indel %	Model Fit (R2)	Knock-out Score
WM46 wtZIP9 gRNA 3. Clone 3.3	0	1	0
WM46 koZIP9 gRNA 3. Clone 3.2	92	0.92	92
WM46 wtZIP9 gRNA 3. Clone 4.6	0	1	0
WM46 koZIP9 gRNA 4. Clone 4.b	90	0.92	90
YUMM1.7 koZIP9 gRNA 3. Clone 3.3	90	0.9	90

Fig. S3. A. Table shows the knock-out scores for WM46 isogenic clones obtained using ICE Analysis software (Synthego). **B.** Blast alignment of the DNA sequences surrounding the gRNA target sequence and SLC39A9 (Ensmbl. Homo Sapiens_SLC39A9_202) are shown for each isogenic clone. As control for the sequencing, WM46 parental cells were sequenced and aligned with human SLC39A9 (Ensmbl. Homo Sapiens_SLC39A9_202). Query = SLC39A9_202; Sbjct

871 = isogenic clone sequences **C.** Target sequence of YUMM1.7 isogenic clone was aligned with
872 *mus musculus* Slc30a9 sequence**. D.** Western blot showing ZIP9 expression in wild type and
873 knock-out YUMM1.7 isogenic clones. **E.** Relative proliferation (cell number) of YUMM1.7
874 wtZIP9 and ΔZIP9 in the presence of 100 nM testosterone (T) for 6 days. The graphs represent
875 the average of three independent experiments. Error bars represent standard error of the mean
876 (SEM). * p value≤0.05. **F.** Immunocytochemistry in WM46 isogenic clones transduced with
877 control pRRL lentivector (E.V.) or hZIP9 expressing lentivector. Western blots below show the
878 proteins in each sample 72 hours after transduction. **G.** Relative cell proliferation (cell number)
879 with testosterone treatment (100 nM) for 7 days in WM46 ΔZIP9 isogenic clones transduced
880 with empty pRRL lentivector (E.V.) (left panel) or pRRL_hZIP9 expressing vector (right panel).
881 Error bars represent standard error of the mean (SEM).
882 **** p value≤0.0001; n.s>0.05.
883
884
885
886
887
888
889
890
891
892
893
894
895
896
897
898
899
900
901
902

Supplementary Figure 4

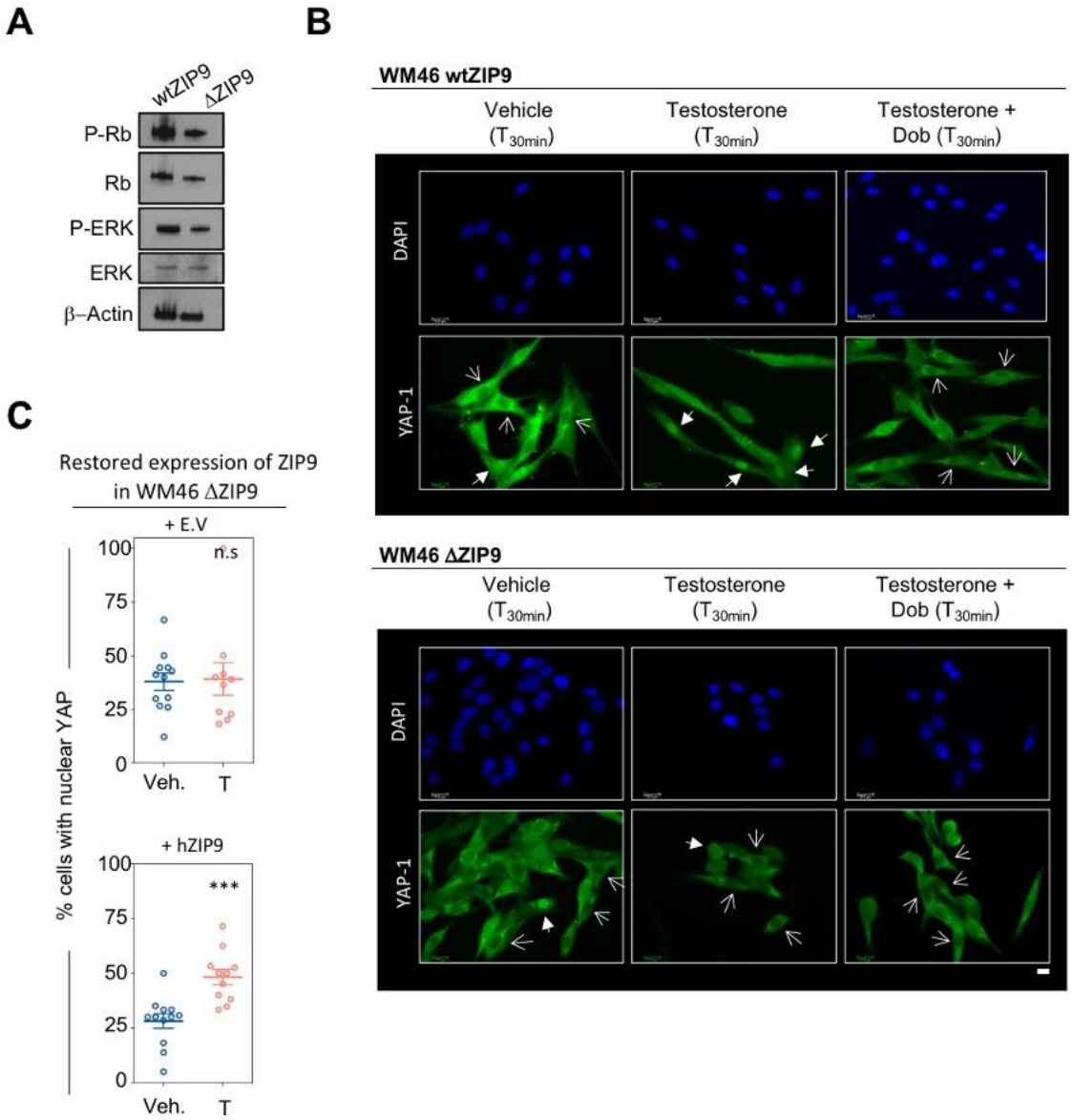

Fig. S4. A. Western blot showing baseline levels of ERK phosphorylation in wtZIP9 and ΔZIP9 WM46 cells. **B.** Representative images of YAP-1 immunodetection after 30 minutes of exposure to 100 nM testosterone (T) +/- 8μM dobutamine (Dob) in wtZIP9 and ΔZIP9 cells. YAP1 is shown in green; β-actin is shown in red; DAPI highlights nuclear DNA in blue. Thin arrows indicate cells where YAP1 is not localized inside the nucleus. Opaque arrows indicate cells with

910 nuclear YAP-1. Scale bar=15μm. **C.** Percentage of WM46 wtZIP9 and ΔZIP9 cells transduced

911 with pRRL empty vector (E.V.) or pRRL_hZIP9 expressing vector with nuclear localization of

912 YAP1. Cells were treated with vehicle and 100 nM testosterone.

913 *** p value≤0.001; n.s>0.05.

914

915

916

917

918

919

Supplementary Figure 5

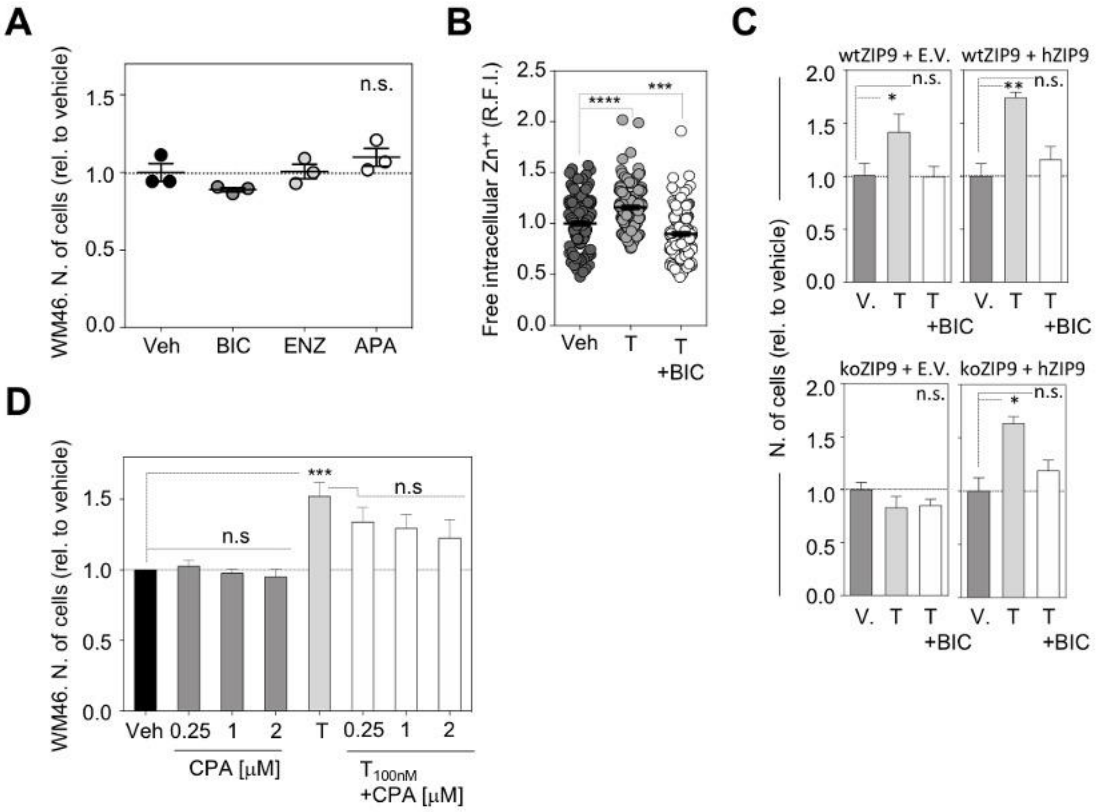

920

921 **Fig. S5. A.** Relative cell proliferation (cell number) in human-derived melanoma cells (WM46)
922 treated with 2μM AR inhibitors (BIC: Bicalutamide; ENZ: Enzalutamide; APA: Apalutamide).
923 **B.** Intracellular Zn^{++} in WM46 cells treated with 100 nM testosterone and/or 2 μM bicalutamide
924 (BIC). **C.** Relative cell proliferation (cell number) of WM46 wtZIP9 and ΔZIP9 transduced with
925 pRRL empty vector (E.V.) or pRRL_hZIP9 expressing vector. Cells were treated with vehicle
926 (V) or 100 nM testosterone +/- bicalutamide (2μM) **D**. Relative cell proliferation of WM46 cells
927 treated with 100nM testosterone and/or cyproterone acetate (CPA) for 6 days.
928 **** p value≤0.0001; *** p value≤0.001; ** p value≤0.01; * p value≤0.05; n.s>0.05.

Supplementary Figure 6

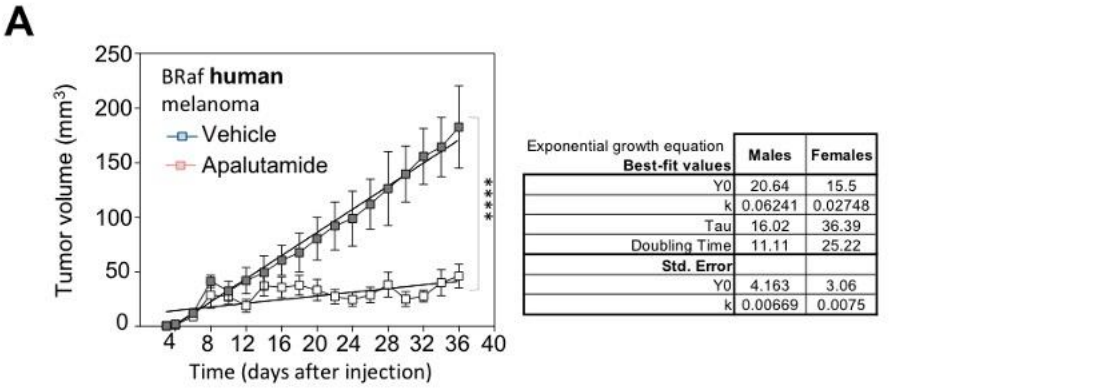

Exponential growth equation Best-fit values	Males	Females
Y0	20.64	15.5
k	0.06241	0.02748
Tau	16.02	36.39
Doubling Time	11.11	25.22
Std. Error		
Y0	4.163	3.06
k	0.00669	0.0075

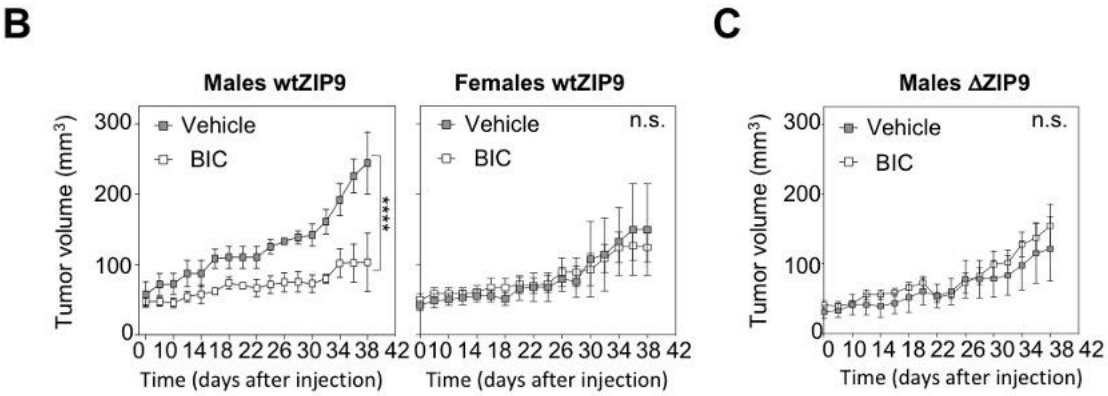

	Vehicle	BIC
Y0	41.04	38.86
k	0.04079	0.02272
Tau	24.52	44.02
Doubling Time	16.99	30.51
Std. Error		
Y0	4.767	5.274
k	0.003447	0.00439

	Vehicle	BIC
Y0	32.77	29.35
k	0.03193	0.03146
Tau	31.32	31.79
Doubling Time	21.71	22.03
Std. Error		
Y0	5.011	5.564
k	0.006338	0.00787

	Vehicle	BIC
Y0	33.3	26.63
k	0.03102	0.03684
Tau	32.24	27.14
Doubling Time	22.34	18.81
Std. Error		
Y0	5.106	6.697
k	0.005979	0.00958

Fig. S6. A. Non-lineal regression analysis (Exponential fit) for males treated with vehicle vs. APA. Doubling time for tumor growth: Vehicle treated males=16.0 days and APA treated males=36.4 days. Linear regression analysis for slope comparison demonstrate significant differences between vehicle treated and apalutamide treated males (p-value<0.0001). **B**. Tumor growth in mice bearing WM46 derived subcutaneous tumors. Linear regression analysis of slopes demonstrates significant differences between vehicle treated and Bic treated males. **C**. Tumor growth in SCID male mice bearing ΔZIP9 WM46 melanoma. Mice were treated daily

937 with bicalutamide (30 mg/kg/day) or vehicle via oral gavage. Exponential fit analyses are

938 included bellow each tumor growth graphical representation.

939 **** p value≤0.0001; n.s>0.05.

940
941
942
943
944
945
946
947
948
949
950
951
952
953
954
955
956
957
958
959
960
961
962
963
964
965
966
967

Supplementary Figure 7

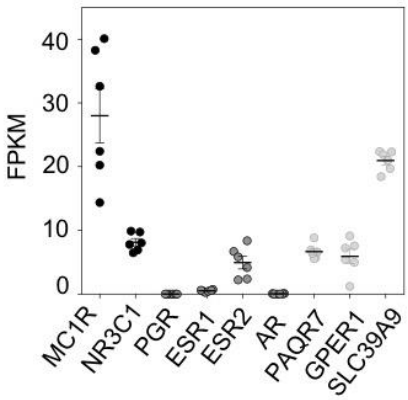

968
969 **Fig. S7.** RNA-seq data from 6 different primary melanocyte cell lines reported as median FPKM
970 (number Fragments Per Kilobase of exon per Million reads). Melanocytic Receptor 1 (MC1R)
971 and Glucocorticoid Receptor (NR3C1) were used as positive controls for membrane and nuclear
972 receptors respectively. PGR: Progesterone Receptor. ESR1: Estrogen Receptor 1. ESR2:
973 Estrogen Receptor 2. PAQR7: Progestin and AdipoQ Receptor Family Member 7. GPER1: G
974 Protein-Coupled Estrogen Receptor 1.
975
976
977
978
979
980

Supplementary Figure 8

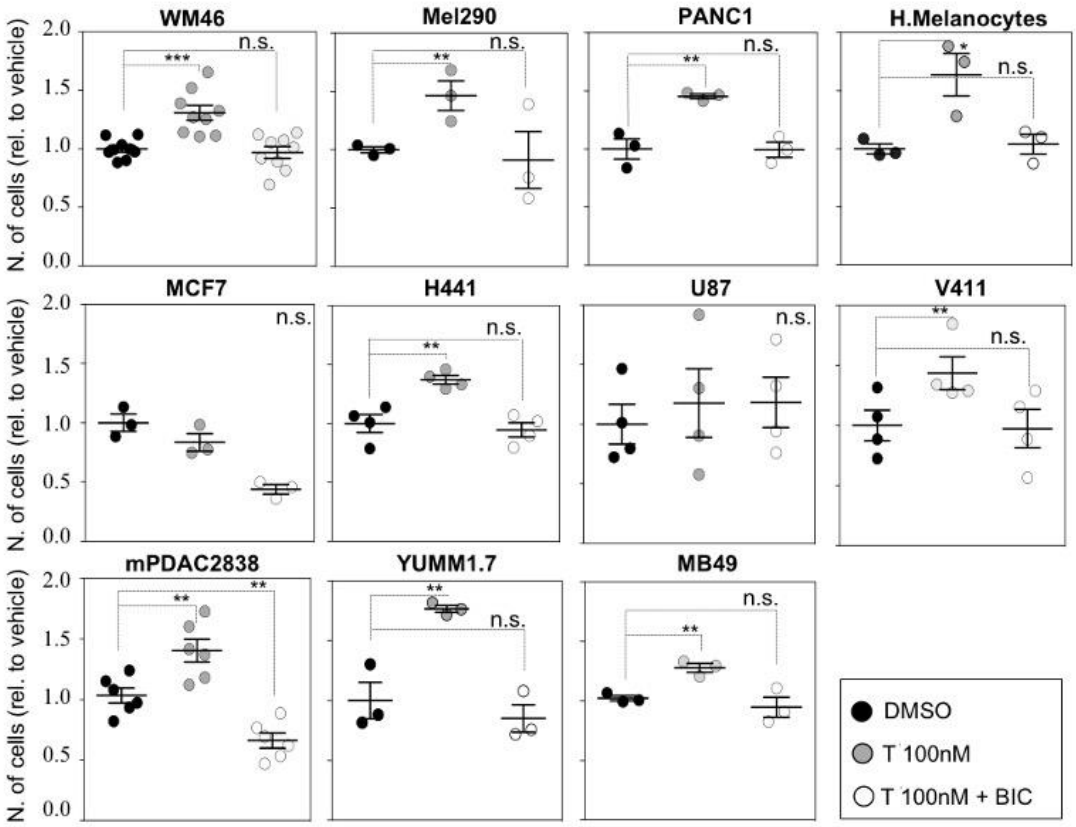

Cell types

WM46: Human skin melanoma
Mel290: Human uveal melanoma
YUMMS1.7: Murine skin melanoma
PANC1: Human pancreatic adenocarcionma
mPDAC: Murine pancreatic adenocarcinoma
MCF7: Human breast cancer
MB49: Mouse bladder cancer
H441: Human lung adenocarcionma
U87: Human glioblastoma
V411: Human adult acute myeloid leukemia

Fig. S8. Relative cell proliferation of a battery of cell lines derived from diverse tumor types in response to 100nM testosterone +/- bicalutamide treatment (2μM).

*** p value≤0.001; ** p value≤0.01; * p value≤0.05; n.s>0.05.